



**HAL**  
open science

## **A review of the LATEX project: mesoscale to submesoscale processes in a coastal environment**

Anne Petrenko, Andrea M. Doglioli, Francesco Nencioli, Marion Kersalé,  
Ziyuan Hu, Francesco d'Ovidio

### ► **To cite this version:**

Anne Petrenko, Andrea M. Doglioli, Francesco Nencioli, Marion Kersalé, Ziyuan Hu, et al.. A review of the LATEX project: mesoscale to submesoscale processes in a coastal environment. *Ocean Dynamics*, 2017, 24 (3), pp.513-533. 10.1007/s10236-017-1040-9 . hal-01505797

**HAL Id: hal-01505797**

**<https://amu.hal.science/hal-01505797>**

Submitted on 11 Apr 2017

**HAL** is a multi-disciplinary open access archive for the deposit and dissemination of scientific research documents, whether they are published or not. The documents may come from teaching and research institutions in France or abroad, or from public or private research centers.

L'archive ouverte pluridisciplinaire **HAL**, est destinée au dépôt et à la diffusion de documents scientifiques de niveau recherche, publiés ou non, émanant des établissements d'enseignement et de recherche français ou étrangers, des laboratoires publics ou privés.

1 **A review of the LATEX project: mesoscale to**  
2 **submesoscale processes in a coastal environment.**

3 **A.A. Petrenko · A.M. Doglioli ·**  
4 **F. Nencioli · M. Kersalé · Z.Y. Hu ·**  
5 **F. d'Ovidio**

6  
7 the date of receipt and acceptance should be inserted later

8 **Abstract** The main objective of the LAgrangian Transport EXperiment (LA-  
9 TEX) project was to study the influence of coastal mesoscale and submesoscale  
10 physical processes on circulation dynamics, cross-shelf exchanges and biogeo-  
11 chemistry in the western continental shelf of the Gulf of Lion, Northwestern  
12 Mediterranean Sea. LATEX was a five-year multidisciplinary project based on  
13 the combined analysis of numerical model simulations and multi-platform field  
14 experiments. The model component included a ten-year realistic 3D numer-  
15 ical simulation, with a 1 km horizontal resolution over the gulf, nested in a  
16 coarser 3 km resolution model. The *in situ* component involved four cruises,  
17 including a large-scale multidisciplinary campaign with two research vessels  
18 in 2010. This review concentrates on the physics results of LATEX, address-  
19 ing three main subjects: 1) the investigation of the mesoscale to submesoscale

---

A.A.Petrenko  
Aix Marseille Université, Université de Toulon, CNRS, IRD, Mediterranean Institute of  
Oceanography (MIO), Marseille, France  
Tel.: +00(33)4 86 09 06 06  
E-mail: anne.petrenko@mio.osupytheas.fr

A.M.Doglioli  
Aix Marseille Université, Université de Toulon, CNRS, IRD, Mediterranean Institute of  
Oceanography (MIO), Marseille, France

F. Nencioli  
Remote Sensing Group, Plymouth Marine Laboratory, Plymouth, Great Britain

M. Kersalé  
Department of Oceanography, Marine Research Institute, University of Cape Town, Rondebosch, South Africa

Z.Y. Hu  
Jiaozhou Bay Marine Ecosystem Research Station, Institute of Oceanology, Chinese  
Academy of Sciences, Qingdao, China

F. d'Ovidio  
Sorbonne Université (UPMC, Paris 6)/CNRS/IRD/MNHN, Laboratoire d'Océanographie  
et du Climat (LOCEAN), Institut Pierre Simon Laplace (IPSL), Paris, France

1 processes. The eddies are elliptic, baroclinic and anticyclonic; the strong ther-  
2 mal and saline front is density-compensated. Their generation processes are  
3 studied; 2) the development of sampling strategies for their direct observa-  
4 tions. LATEX has implemented an adaptive strategy Lagrangian tool, with a  
5 reference software available on the web, to perform offshore campaigns in a La-  
6 grangian framework; 3) the quantification of horizontal mixing and cross-shelf  
7 exchanges. Lateral diffusivity coefficients, calculated in various ways including  
8 a novel technique, are in the range classically encountered for their associated  
9 scales. Cross-shelf fluxes have been calculated, after retrieving the near-inertial  
10 oscillation contribution. Further perspectives are discussed, especially for the  
11 ongoing challenge of studying submesoscale features remotely and from *in situ*  
12 data.

13 **Keywords** mesoscale · submesoscale · Lagrangian · Gulf of Lion · North-  
14 western Mediterranean Sea · cross-shelf flux

## 15 1 Introduction

16 Coastal waters, in spite of their small surfaces and volumes (8% and 0.05% of  
17 the global ocean, respectively), are currently the object of crucial questions.  
18 This environment is the link between the continents, highly impacted by hu-  
19 man presence and activities (40% of the world population lives less than 100  
20 km from the coast) and the ocean, one of the main regulators of the global ther-  
21 mal and biogeochemical cycles. The coastal zone is usually characterized by  
22 high biological productivity due to a large availability in nutrients coming from  
23 human and river inputs. Thus coastal areas contribute to an important part  
24 of the carbon sequestration in the ocean and play a key role in climate change.  
25 Moreover, coastal dynamics have strong ecological repercussions, such as the  
26 regulation of biogeochemical cycles through local circulation and cross-shelf  
27 exchanges, as well as the dispersion of larvae and pollutants through current  
28 advection. Coastal physical processes also influence higher trophic levels hav-  
29 ing, for example, repercussions for fisheries. Their understanding is therefore  
30 of critical importance for sustainable management of the marine environment.  
31 Among coastal physical processes, mesoscale and submesoscale -hereafter re-  
32 ferred to as (sub)mesoscale- processes have a particularly important role.

33 (Sub)mesoscale processes are ubiquitous in the open ocean, as well as in  
34 coastal waters. They have spatial scale of the order of few kms and tempo-  
35 ral scales of days to weeks, hence they are typically localized and ephemeral.  
36 On one hand, mesoscale processes are generally produced by the instability  
37 of large scale currents (McWilliams et al., 1983; Robinson, 1983). They are  
38 in approximate geostrophic balance in the horizontal and hydrostatic balance  
39 in the vertical, and are characterized by small Rossby and Froude numbers  
40 (Cushman-Roisin, 1994). Thus, their dynamics are predominantly horizontal.  
41 Submesoscale processes, on the other hand, usually arise from instabilities in  
42 the mixed layer due to mesoscale-induced stirring, wind forcing, or a com-  
43 bination of the two (e.g. Thomas et al., 2008). They are characterized by

$\mathcal{O}(1)$  Rossby and Richardson numbers. Thus, they are typically ageostrophic, and their dynamics markedly 3D. They can generate non negligible vertical motion and enhance local mixing. Hence submesoscale processes can have an important biogeochemical impact by supplying nutrients both vertically and laterally (Moore II et al., 2007; Suthers et al., 2011; Mahadevan, 2016). Length scales of mesoscale oceanic processes in coastal area are usually of  $\mathcal{O}(10 - 100)$  km, while those of submesoscale processes of  $\mathcal{O}(0.1 - 10)$  km. (Sub)mesoscale processes such as coastal eddies, fronts and filaments are particularly important for coastal environments since they are key contributors to the energy budget, tracer transport and biogeochemical cycles. This Review focuses on the first two contributions.

Coastal eddies have generally been related to strong currents, mixed layer stratification and/or wind forcing (Mitchelson-Jacob and Sundby, 2001), outflows of coastal waters (Crawford, 2002; Di Lorenzo et al., 2005), flow instabilities along the continental slope (Melson et al., 1999; Flexas et al., 2002), topographic forcing (MacFadyen et al., 2008; Staneva et al., 2001), upwelling processes (MacFadyen and Hickey, 2010) or transfers of energy from other eddies (Garreau et al., 2011).

Fronts are regions characterized by strong horizontal gradients of hydrographic properties (temperature, salinity or both). Typically, the variations of a parameter across the front axis are an order of magnitude larger than changes of this parameter over the same distance on either side of the front. If the horizontal gradients of temperature and salinity are also associated with variations in density, the front is named a density front. While if the horizontal temperature gradient is balanced by that of salinity, so that the resulting cross-front density profile is almost constant, the front is called density-compensated. Fronts are linked to mesoscale dynamics because they are often created by mesoscale-induced stirring, although other processes can also generate them: e.g. tides, atmospheric forcing, freshwater inputs. They can also be linked to submesoscale dynamics, because the front's development often leads to, or is associated with the formation of 3D secondary ageostrophic circulation (Thomas et al., 2008; Capet et al., 2008b).

Coastal eddies and fronts have a strong influence on horizontal ocean mixing and, hence, could impact diffusivity. In the past, *in situ* estimates of lateral diffusivity at scales smaller than 100 km have been most commonly obtained from passive tracer (e.g. sulfur hexafluoride,  $SF_6$ ) experiments. Such estimates are based on the hypothesis that, under local mesoscale stirring (which can be approximated, to a first order, as 2D and hence divergence-free), the width of the patch decreases until the effects of mesoscale stirring are balanced by smaller scale diffusion and an equilibrium is reached. Thus, lateral diffusivity can be computed by combining estimates of the strain rate (usually estimated from successive *in situ* mappings Ledwell et al. 1998, or from the analysis of satellite imagery of surface tracers, Abraham et al. 2000) with *in situ* measurements of the patch width. Lateral diffusivities computed using this approach range from 0.5 to 25  $m^2 s^{-1}$  for tracer filaments with widths between 1 and 10 km. At similar scales but in less energetic systems, lateral diffusivities have

1 also been estimated by neglecting the strain and measuring the growth of  
2 the roughly circular tracer patch (e.g. the Santa Monica Basin Tracer Exper-  
3 iment, Ledwell and Watson 1991, and the BATRE experiment, Holtermann  
4 et al. 2012). Following this method, the lateral diffusivities were of the order  
5 of  $10 \text{ m}^2 \text{ s}^{-1}$  for the interior of the two basins at scales on the order of  $10 \text{ km}$ .

6 Eddies and fronts can also have an important role on cross-shelf exchanges.  
7 In the last decades, cross-shelf exchanges have been the focus of several stud-  
8 ies (Brink and Cowles, 1991; Biscaye, 1994; Huthnance et al., 2002; Johnson  
9 and Chapman, 2011). Continental shelves are often bounded by strong large-  
10 scale (geostrophic) currents flowing along the steep bathymetry of the shelf  
11 edge (Huthnance, 1995). These tend to inhibit cross-shelf exchanges which,  
12 therefore, are mainly enabled by localized, mostly short-lived and predom-  
13 inantly ageostrophic events, such as internal tide breaking (Hopkins et al.,  
14 2012), Ekman transport (Kirincich and Barth, 2009), dense shelf water cas-  
15 cading (Canals et al., 2006), eddies (Capet et al., 2008a; Nagai et al., 2015),  
16 mesoscale-stirred fronts (Ferrari, 2011) and filaments (Nagai et al., 2015). Es-  
17 timates of the net fluxes induced by these processes remain hard to quan-  
18 tify from *in situ* observations due to the temporal and spatial scales of the  
19 processes involved (Huthnance et al., 2009). In global models, the effect of  
20 (sub)mesoscale processes is still parametrized (e.g. eddy viscosities and dif-  
21 fusivities). Indeed, despite some recent advancements towards (sub)mesoscale  
22 resolving resolutions, they usually cannot properly resolve their associated dy-  
23 namics. Nonetheless, (sub)mesoscale processes can now be accurately resolved  
24 by high-resolution regional numerical models. Therefore, the impact of these  
25 processes on coastal environments and cross-shelf exchanges has been investi-  
26 gated at the regional scale mainly through the analysis of numerical simula-  
27 tions with relatively rare concomitant observations for comparisons (Burchard  
28 et al., 2008; Capet et al., 2008a,b). For these reasons, direct observations of  
29 (sub)mesoscale processes still represent a key and much-needed component for  
30 the further advancement of both regional and global models.

31  
32 The main objective of the LAgrangian Transport EXperiment (LATEX)  
33 project was to study the influence of coastal (sub)mesoscale physical processes  
34 on circulation dynamics, cross-shelf exchanges and biogeochemistry in the  
35 western continental shelf of the Gulf of Lion (GoL), Northwestern Mediter-  
36 ranean sea (Fig. 1). LATEX was a five-year (2007-2011) multidisciplinary  
37 project based on the combined analysis of numerical model simulations and  
38 multi-platform field experiments.

39 The GoL is a large continental shelf, approximately the shape of a semi-  
40 circle with a radius near  $100 \text{ km}$ , and a surface area of about  $11000 \text{ km}^2$ .  
41 The main forcings of the shelf circulation include: (i) the strong northerly and  
42 northwesterly continental winds (the Mistral and the Tramontane); (ii) the  
43 Northern Current (hereafter NC) which represents the northern branch of the  
44 large-scale cyclonic circulation of the western Mediterranean basin, flowing  
45 along the continental slope from the Ligurian Sea to the Catalan Sea (Millot,  
46 1990); (iii) the Rhône River which is the main fresh water source of the GoL.

1 A general description of the hydrodynamics of the GoL is provided by Millot  
2 (1990). The existence of an anticyclonic circulation in the western part of the  
3 gulf following upwelling phenomena and an offshore drift of surface water has  
4 been first hypothesized in Millot (1979, 1982). Later, Estournel et al. (2003)  
5 showed an anticyclonic eddy located at the center of the GoL continental shelf  
6 or an anticyclonic circulation covering the western and center parts of the  
7 GoL, using both observations and model. On the eastern part of the GoL  
8 continental shelf, eddies are generated by the local wind (Allou et al., 2010;  
9 Schaeffer et al., 2011). (Sub)mesoscale processes are quite active also offshore  
10 the GoL, where submesoscale coherent vortices can be formed in regions of  
11 deep convection (Bosse et al., 2016).

12 The GoL is particularly appropriate for studying coastal mesoscale dynam-  
13 ics and its role in regulating cross-shelf exchanges. Before the LATEX cam-  
14 paigns, two processes were recognized as main contributors to the exchanges  
15 between the GoL and offshore waters: dense shelf water cascading (Durrieu  
16 et al., 2013; Canals et al., 2006) and more shallow processes associated with  
17 the NC (Millot and Taupier-Letage, 2005). Intrusions of the NC on the con-  
18 tinental shelf of the GoL have been studied in the western (Millot and Wald,  
19 1980; Petrenko et al., 2008), central (Estournel et al., 2003; Petrenko, 2003)  
20 and eastern parts (Petrenko et al., 2005; Barrier et al., 2016) of the GoL. On  
21 the eastern side, the flux of some of these intrusion events were estimated  
22 with *in situ* data, ranging between 0.37 Sv (Petrenko et al., 2013) and 0.5  
23 Sv (Petrenko et al., 2005). By 2006, some (sub)mesoscale processes had been  
24 identified and studied on the eastern side of the GoL (Petrenko et al., 2005)  
25 and in its central region, especially linked to the Rhône river plume (Naudin  
26 et al., 1997; Broche et al., 1998). However, in the western part of the GoL, the  
27 focus had been mainly on dense water formation (Durrieu De et al., 2005),  
28 while smaller scale processes had been relatively poorly investigated. The LA-  
29 TEX project aimed at filling this gap, addressing -in its physics component-  
30 three main questions:

- 31 – What are the generation mechanisms and the general characteristics of
- 32 (sub)mesoscale processes in the western GoL?
- 33 – How can field experiments be designed to investigate coastal (sub)mesoscale
- 34 structures ?
- 35 – How much horizontal mixing and cross-shelf exchanges are associated with
- 36 these processes?

37  
38 After a brief introduction to the LATEX project (section 2), this review will  
39 provide answers to these questions. Each question will be addressed in one  
40 specific section: dynamics in the western GoL (section 3), *in situ* sampling  
41 strategies (section 4), calculation of horizontal mixing and exchanges (sec-  
42 tion 5). Finally, the Conclusion and Perspectives are drawn in section 6 and  
43 7, respectively.

## 2 Data and Methods

Numerical model simulations and *in situ* observations from a series of field experiments enabled us to answer the three main questions raised above.

### 2.1 Numerical modeling

The LATEX project included a numerical component whose initial objective, during the pilot phase, was to study the probability of occurrence of stable mesoscale structures in the GoL (Hu et al., 2009). Once this was positively achieved, the modeling component aimed at two main objectives: 1) to investigate the mechanism of formation and the characteristics of these structures; 2) to provide additional information to integrate/complement the analysis from *in situ* observations.

The model used in the project was Symphonie (Marsaleix et al., 2006, 2008), a 3D primitive equation, free surface, sigma coordinate ocean model, based on the Boussinesq and hydrostatic approximations. Components of current, temperature and salinity are computed on an Arakawa-C grid using a classic finite difference method. The vertical turbulence closure is achieved through a prognostic equation for the turbulent kinetic energy and a diagnostic equation for the mixing and dissipation length scales (Gaspar et al., 1990). As part of the pilot LATEX project in 2007, an optimized configuration of the Symphonie model was established for the Northwestern Mediterranean Sea (3 km resolution), with a nested high-resolution (1 km) model in the GoL (Hu et al., 2009). The high-resolution model domain is shown in Fig. 1.

Using this configuration, a realistic simulation was performed over 10 years, from 2001 to 2010. The initial and open boundary conditions for the larger domain were provided by the Mediterranean Forecasting System (MFS, <http://eurogoos.eu/member-product/mediterranean-ocean-forecasting-system/>) general circulation model (Pinardi, 2003) with a resolution of  $1/8^\circ$ . The atmospheric forcing was obtained from the 3-hr outputs of the meteorological model Aladin of Météo-France with a spatial resolution of  $0.1^\circ \times 0.1^\circ$ . The daily fresh water fluxes from the major rivers were taken into account. No data assimilation was included in the simulation. The readers are referred to Hu et al. (2009, 2011a) for more details about the model settings.

The simulation was used to characterize the stable mesoscale processes in the western part of the GoL. The utility program WATERS (Doglioli et al., 2007) was used to objectively identify and follow coherent eddy structures. The method is based on wavelet analysis of horizontal slices of modeled relative vorticity. It detects the contour and the center of a coherent structure and monitors its characteristics over time and space. The numerical outputs also provided information on the larger scale dynamical context of the processes taking place before, during and after the field cruises.

## 2.2 Satellite derived products

Satellite data include SeaWiFs chlorophyll concentration (from NASA Goddard Space Flight Center) and a pseudo-SST (Sea Surface brilliance Temperature provided by Météo-France and corresponding to channel 4 of the AVHRR sensor: Advanced Very High Resolution Radiometer). These were used to identify, and follow in time, the signatures of the (sub)mesoscale processes in chlorophyll concentration and temperature. Surface geostrophic velocities produced by Ssalto/Duacs (Ssalto: ground Segment for multi-missions of altimetry, orbitography and precise location, Duacs: Developing use of altimetry for climate studies,  $1/8^\circ$  resolution over the Mediterranean basin) and distributed by AVISO, with support from CNES (AVISO: Archiving, Validation and Interpretation of Satellite Oceanographic data, CNES: French National Center for Spatial Studies, <http://www.aviso.altimetry.fr/duacs/>) were used for Finite Size Lyapunov Exponent (FSLE) analysis. Detailed description of the processing and corrections of AVISO satellite altimetry can be found in the Ssalto/Duacs User Handbook (2010).

Along with Finite Time Lyapunov Exponents (FTLEs) (Haller and Yuan, 2000), FSLEs (Aurell et al., 1997) have recently emerged as a powerful Lagrangian diagnostic for the investigation of the dispersion properties of a flow. Both methods measure the separation rate of the trajectories of close initial particles, and can be applied for two complementary goals: quantifying dispersion processes (Waugh and Abraham, 2008; Haza et al., 2010; Lumpkin and Elipot, 2010; Schroeder et al., 2011), or mapping Lagrangian Coherent Structures (LCSs) (Haller and Yuan, 2000; d'Ovidio et al., 2004; Olascoaga et al., 2006; Lehahn et al., 2007; Beron Vera et al., 2008; Haller, 2011). Repulsive and attractive LCSs are associated with hyperbolic points of the flow, and provide direct information on transport and mixing patterns (Mancho et al., 2008): particles spread while moving toward hyperbolic points along repelling LCSs, whereas they aggregate while moving away from hyperbolic points along attracting LCSs, which thus represent transport barriers (Lehahn et al., 2007; Haller, 2011). The spatial organization of these structures has a large impact on the coastal environment, not only because they influence the dispersion of any tracer in the water, but also because, by separating dynamically distinct regions of the flow, they can define fluid dynamical niches which contribute to the structuring of marine ecosystems (d'Ovidio et al., 2010) and top predator distribution (Tew Kai et al., 2009; Cotté et al., 2011; De Monte et al., 2012). Generally this altimetry based approach is less reliable in coastal regions, where the different ageostrophic dynamics induced by boundaries and nearshore forcings (Csanady, 1982), insufficient sampling, presence of land mass and inaccuracy of geophysical corrections (Bouffard et al., 2008) represent critical limiting factors for altimetry. For this reason, during the campaign of September 2010 (see section 2.3), daily maps of FSLEs were produced from real-time maps of absolute dynamic topography as a first guess of transport barriers and frontal systems, which were then precisely located by an adaptive strategy. The altimetry-derived FSLE maps, used in Nencioli et al. (2011,

1 2013, 2016) and in this current review paper, were re-processed after the cam-  
 2 paign using the delayed-time maps of absolute topography. The near-real time  
 3 and delayed-time products did not show large differences in the study area.

#### 4 2.3 Field experiments

5 The LATEX project involved four cruises:

- 6 – Latex00, a preliminary three-day test cruise (June 9-11, 2007), (Petrenko,  
 7 2007);
- 8 – Latex08, a one-week cruise to study an eddy (Sept. 1-6, 2008), (Petrenko,  
 9 2008);
- 10 – Latex09, a one-week cruise dedicated to study another eddy (Aug. 25-30,  
 11 2009), (Petrenko, 2009);
- 12 – Latex10, a tracer, multidisciplinary cruise conducted from two R/Vs (Sept.  
 13 1 - 24, 2010), (Petrenko, 2010).

14 Note that, in the nomenclature for the cruises: LatexYY, YY indicates the  
 15 year of the cruise for the second to the fourth cruise. The initial pilot cruise  
 16 kept its original official name: Latex00, despite having taken place in 2007.

17 *Latex08 & Latex09* - These two LATEX field cruises focused on the detection  
 18 and study of coastal mesoscale structures (Hu et al., 2011b; Kersalé et al.,  
 19 2013). They took place on board the R/V Téthys II. A VMBB-150 KHz ship-  
 20 based Acoustic Doppler Current Profiler (ADCP) was used to measure current  
 21 velocities every 4 meters down to 247 m depth (see Petrenko et al. 2005 for  
 22 details). At chosen stations, profiles were collected using a SeaBird SBE 19  
 23 conductivity-temperature-depth (CTD) sensor. During Latex08, since the sea  
 24 state did not allow use of the CTD, temperature profiles were obtained by  
 25 using XBTs (eXpendableBathyThermographs). In addition, sea surface tem-  
 26 perature, salinity, and fluorescence were measured continuously at the surface  
 27 by the ship thermosalinograph SBE 21. Wind was measured at 10 m above  
 28 the surface. Technocean Surface Velocity Program (SVP) subsurface drifters,  
 29 equipped with a 6 m long holey-sock drogue extending between 12 m and 18 m,  
 30 were deployed in the eddy to track the fluid motion at 15 m depth. Drifter  
 31 positions were provided by the Argos system in quasi-real-time.

32 *Latex00 & Latex10* - These other two LATEX field campaigns were dedicated  
 33 to a tracer release experiment.

34 The first one, Latex00, was part of a pilot project which aimed to demon-  
 35 strate the feasibility of our Lagrangian methodology and of a  $SF_6$  tracer ex-  
 36 periment in the GoL. To our knowledge, at the time of LATEX, only one  $SF_6$   
 37 tracer experiment had taken place in a coastal environment (Wanninkhof et al.,  
 38 1997).  $SF_6$  is a gaseous electrical insulator with a very low solubility in seawater,  
 39 which results in a background concentration in the seawater of about 0.3  
 40  $\text{fmol l}^{-1}$  ( $\text{fmol} = 10^{-15} \text{ mol}$ ).  $SF_6$  can be detected at these low concentrations

1 using the high sensitivity of gas chromatography with an electronic capture  
2 detector (Law et al., 1994). During Latex00, the background concentrations  
3 of  $SF_6$  were measured in the surface mixed layer of the GoL. The values were  
4 around  $1.35 \text{ fmol l}^{-1}$ , which is the concentration of  $SF_6$  expected for seawater  
5 in equilibrium with the atmosphere. Therefore, during the Latex10 cruise, it  
6 was possible to use a volume of  $4 \text{ m}^3$  of seawater saturated with  $SF_6$  to release  
7 a patch of  $50 \text{ km}^2 \times 50 \text{ m}$ , with  $SF_6$  concentrations roughly 200 times higher  
8 than the background value.

9 The main goal of the last field experiment, Latex10, was to analyze the  
10 transport patterns and dispersion rates induced by a mesoscale structure  
11 within the Lagrangian reference frame associated with it. Therefore, the ex-  
12 periment was designed to combine the release of  $SF_6$  with the deployment of  
13 an array of Lagrangian buoys. Latex10 involved the coordination of two R/Vs,  
14 one (the *R/V Le Suroît*) dedicated to the  $SF_6$  experiment and the other one  
15 (the *R/V Téthys II*) dedicated to the survey of the underlying (sub)mesoscale  
16 processes. To successfully monitor such processes, the sampling strategy of the  
17 *R/V Téthys II* was routinely optimized and adapted (hence “adaptive strat-  
18 egy”) in a Lagrangian framework based on the near-real time analysis of all the  
19 available *in situ*, remote or modeled data (see also section 4). *In situ* measure-  
20 ments collected by the *R/V Téthys II* were similar to the ones during Latex09  
21 (see above). In addition, turbulence profiles, down to 50 m, were acquired with  
22 a SCAMP (Self-Contained Autonomous Microstructure Profile). Lagrangian  
23 SVP subsurface drifters were released from both the *R/V Téthys II* and the  
24 *R/V Le Suroît*. Some were captured afterwards in order to be redeployed ac-  
25 cording to the near real-time analysis of LCSs (see Nencioli et al. (2011) for  
26 more details). The tracer release and mapping were performed from the *R/V*  
27 *Le Suroît*. The strategy was defined in coordination with the *R/V Téthys II*  
28 based on the Lagrangian navigation software (see subsection 4.3). On the *R/V*  
29 *Le Suroît*, a VMBB-150 KHz hull-mounted ADCP provided current velocities  
30 every 8 meters when depth was superior to 300 m or every 4 meters in shallow  
31 waters. As on the *R/V Téthys II*, the *R/V Le Suroît* thermosalinograph mea-  
32 sured surface temperature, salinity and fluorescence along the ship transects.  
33 Wind was measured at 18 m above the surface. Numerous biogeochemical and  
34 biological measurements were also collected by the *R/V Le Suroît*, but their  
35 analysis is beyond the scope of this physics review paper. Up to three gliders  
36 were coordinated (L. Mortier and P. Testor, LOCEAN, Paris; L. Beguery, DT  
37 INSU, La Seyne sur Mer, France) to circulate in the zone at the time of the  
38 study. Their positions, and derived current velocities along their routes, were  
39 sent in near real-time to the two R/Vs to provide a global view of the general  
40 circulation around the study area. The analysis of the current, temperature  
41 and salinity fields produced by the MFS was also sent to the *R/V Téthys*  
42 *II* to be taken into account in the adaptive strategy. The interested reader  
43 can refer to the two Latex10 cruise reports for additional details (available on  
44 [www.mio.univ-amu.fr/LATEX](http://www.mio.univ-amu.fr/LATEX); Publications section).

### 3 Dynamics in the western GoL

The numerical simulations showed that mesoscale structures were common in the western part of the GoL during stratified conditions. Structures that last more than 15 days were qualified as "long-life" (Hu et al., 2011a). This limit of 15 days was chosen after several sensitivity tests. It represents a typical scale below which, in this coastal area and during stratified conditions, structures are considered submesoscale both temporally and spatially. All long-life features were anticyclonic baroclinic eddies. The results from the numerical simulation were then further investigated to better understand the generation processes and characteristics of these eddies.

The most common process of generation (Hu et al., 2011a) is due to a combined effect of wind forcing and topography, involving upwelling (south of Cape d'Agde) and Ekman transport southwestward (Fig. 2). These last two processes are generally due to strong northwest (NW) wind bursts, lasting more than 3 days. Once an eddy is created, strong stratification allows for a better transfer of wind-induced potential energy to eddy kinetic energy. However, additional strong wind bursts are also required to sustain the eddy in size and intensity. All details about the strength and persistence of the wind forcing can be found in Hu et al. (2011a). The level of stratification was estimated from the Symphonie numerical output by calculating the absolute value of potential energy anomaly,  $\phi$ , throughout the water column of the eddy generation area (hatched area on Fig. 1).  $\Phi$  was shown to be a good indicator of the water column stability (Hu et al., 2011a; De Boer et al., 2008; Burchard and Burchard, 2008). The more stratified the water column, the higher the value of  $\phi$ . The reader can refer to Hu et al. (2011a) for more details on this calculation. Over the ten year simulation (Fig. 3), the stratified conditions were classified into three major categories, according to the range of  $\phi$ :

1. a weak stratification with a value of  $\phi$  below  $20 \text{ J m}^{-3}$ , as during the winter-spring season;
2. an intermediate stratification with a value of  $\phi$  around  $60 \text{ J m}^{-3}$ ; as during early May and late October for all years between 2001 and 2010, along with summers 2002 and 2004;
3. a strong stratification with a value of  $\phi$  reaching  $100 \text{ J m}^{-3}$ , as during all summer seasons except in 2002 and 2004.

When stratification is not high enough, an eddy can be generated but it does not last longer than the time threshold of 15 days, and is classified as transient. The most stratified conditions are observed during the months of July to October (Fig. 3) and coincide with the occurrence of all the long-life eddies modeled in the GoL.

A second generation process has also been identified (Kersalé et al., 2013). This other process requires the presence of a  $\mathcal{O}(100 \text{ km})$  anticyclonic circulation ( $3^\circ - 4^\circ \text{E}$  and  $42^\circ - 43^\circ \text{N}$ ) and a strong meandering of the NC (Fig. 4). The NC pushes the anticyclonic structure towards the coast, squeezing it so that it finally splits into two structures. The northern one, an anticyclonic barotropic

1 eddy similar to the wind-induced eddies previously described, remains in its  
 2 area of formation over the continental shelf. The southern structure, on the  
 3 other hand, does eventually migrate southward to the Catalan basin, con-  
 4 tributing to the cross-shelf exchanges described in more detail in section 5.2.

5 According to the daily numerical outputs, 11 long-life anticyclonic eddies  
 6 have occurred during the 10-year period of the simulation (Fig. 5). They are  
 7 present only during the stratified period from July to October of a given year.  
 8 The mean duration of these eddies is 44.5 days (with a standard deviation of 20  
 9 days), which is long in a rapidly-varying coastal environment such as the GoL.  
 10 Among these 11 vortices, only one was formed by the second process (Kersalé  
 11 et al., 2013), while the other 10 are explained by the first generation process  
 12 (Hu et al., 2011a). Throughout the years, the eddies occurred as follows:

- 13 – years without eddies (2004, 2007),
- 14 – years with 1 eddy (2001, 2002, 2006, 2008 and 2010),
- 15 – years with 2 eddies (2003, 2005 and 2009).

16 Hereafter vortices are called LatexA(i)\_YY, with an A to specify that the eddy  
 17 is anticyclonic, and potentially an i to indicate that this is the i-th eddy of  
 18 year YY for the years with more than one eddy.

19 The years 2004 and 2007 stand out as unusual because they had no long-life  
 20 eddy. In 2004, transient eddies appeared but no long-life eddy ever occurred  
 21 despite successive strong NW wind events, probably due to the weakness of  
 22 the summer stratification (Fig. 3). In 2007, since the stratification was strong  
 23 and the wind forcing was particularly intense, the mesoscale eddy increased in  
 24 scale and became an anticyclonic circulation larger than the study area (see  
 25 Figure 4 of Hu et al. (2011a)). Furthermore, a third year was also found to be  
 26 anomalous. In 2002, a long-life eddy existed despite an intermediate level of  
 27 stratification (Fig. 3). This occurred because, as in 2007, the wind forcing was  
 28 particularly strong, persistent and frequent.

29 Numerical model results have been complemented with *in situ* observations  
 30 from the Latex08 and Latex09 campaigns to study the characteristics of these  
 31 structures (Figure 6). Both datasets showed that these eddies are baroclinic,  
 32 mainly confined within the mixed layer depth (about 30 m), and generally el-  
 33 liptical (Hu et al., 2011a; Kersalé et al., 2013). They have a diameter of about  
 34 20 km and tangential speed of the order of  $0.3\text{-}0.4\text{ m s}^{-1}$  on the outer edge so  
 35 that a full loop around the eddy takes  $\sim 3$  days. When possible, the character-  
 36 istics of the modeled eddies were compared with those measured and showed  
 37 very good agreement (Hu et al., 2011a; Kersalé et al., 2013). For instance,  
 38 the characteristics of the second long-life anticyclonic eddy of 2009, hereafter  
 39 LatexA2\_09, were compared. The center of the eddy was estimated at  $3^{\circ}26'E$   
 40 -  $42^{\circ}36'N$  in the model and at  $3^{\circ}34'E$  -  $42^{\circ}33'N$  from *in situ* velocity cross-  
 41 sections of the eddy (see Section 4.1). The radial distribution of tangential  
 42 velocities (see Fig. 3 of Kersalé et al. 2013 and accompanying text) was also  
 43 used to estimate the region of the eddy in solid-body rotation, and hence its  
 44 horizontal diameter. Tangential velocities linearly increased to average maxi-  
 45 mum values  $V_{max}$  of  $\sim 0.35\text{ m s}^{-1}$ , at radial distances  $R_{max}$  between 9 and 15

1 km. Thus, the *in situ* estimate of eddy dimensions is very close to that from  
 2 the model (mean radius of 14.3 km based on the WATERS wavelet analysis  
 3 described in Section 2.1). Analogously, the eddy vertical extents from model  
 4 and observations were also very close, being 37 m and 35 m, respectively. The  
 5 local Rossby number  $R_o$  and the Rossby radius of deformation  $R_d$  were also  
 6 estimated at 0.26 and 5.9 km, respectively. Since  $R_{max} > R_d$ , this eddy was  
 7 classified as a mesoscale structure. Nonetheless the local Rossby number was  
 8 not small, so its dynamics could not be approximated by quasi-geostrophic  
 9 theory.

10 Coastal dynamics was quite different for the Latex10 campaign in Septem-  
 11 ber 2010, during which no anticyclonic structure was present. AVHRR pseudo-  
 12 SST imagery showed that the circulation in the western part of the GoL was  
 13 characterized by the development of a strong thermal front (Figure 7c). The  
 14 combined analysis of ship-based and Lagrangian observations revealed that  
 15 the front was associated with an intense flow 10 km wide and roughly parallel  
 16 to the coast, through which waters from the continental shelf left the GoL  
 17 towards the Catalan Basin (Nencioli et al., 2011). The front was formed due  
 18 to the convergence, and the resulting stirring, of warmer open Northwestern  
 19 Mediterranean waters, with colder waters on the continental shelf (respec-  
 20 tively, O and C waters in Nencioli et al. 2013, 2016). Analysis of wind data  
 21 and drifter trajectories indicated that the movement of the former was mainly  
 22 driven by the NC dynamics along the continental slope, whereas the latter  
 23 were advected southward out of the GoL due to Ekman flow following strong  
 24 NW wind events.

25 Therefore, the front formation was mainly driven by the stirring induced  
 26 by the interaction between wind-induced and large-scale circulation (Nencioli  
 27 et al., 2016). Analysis of temperature, salinity and density data from cross-  
 28 front transects showed that the front was mostly density-compensated (Nen-  
 29 cioli et al., 2013). Temperature (salinity) gradients could reach up to 2°C  
 30 (0.4 psu) over less than 4 km across the front. The distribution of the vorticity  
 31 Rossby number across the front showed predominant values smaller than  
 32  $\mathcal{O}(1)$ , with occasional maxima around  $\mathcal{O}(1)$  (Nencioli et al., 2016, SI, Fig. 6).  
 33 This indicated that the Latex10 front was mainly associated with geostrophic  
 34 (i.e. mesoscale) dynamics. Therefore, although a surface intensified geostrophic  
 35 flow and stronger vertical velocities may have occasionally occurred where the  
 36 horizontal density gradient and relative vertical vorticity were large, the role  
 37 of the local frontal dynamics was not explored. The implicit assumption is  
 38 that horizontal advection by the geostrophic and Ekman flows that induced  
 39 the formation of the front had stronger impact on the front's dynamics and  
 40 temporal evolution than secondary ageostrophic circulation (Nencioli et al.,  
 41 2013, 2016).

## 4 Design of field experiments to investigate coastal (sub)mesoscale structures

A powerful approach to quantify complex and ephemeral physical coastal processes is to perform the study in a Lagrangian reference frame with an adaptive strategy. This allows for the deconvolution of advection versus dispersion processes. At the time of the submission of the LATEX project to funding agencies, Lagrangian strategies were not as commonly used as now. Together with Griffa et al. (2007), LATEX was a pioneer study in adopting this type of approach. The main three examples of adaptive Lagrangian sampling strategy used during LATEX are presented in the next subsections.

### 4.1 Eddy *in situ* tracking (Latex08 and Latex09 - *R/V Téthys II*)

During Latex08 and Latex09, a methodology to identify, follow and *in situ* sample an eddy, was developed, tested and improved. Before the cruise, analysis of pseudo-SST and ocean color satellite imagery was used to identify the presence of mesoscale eddies. If an eddy was detected, its center and potential translation speed were estimated with these data. This information was compared to and integrated with the results from the numerical simulations described in Section 2.1. The results were used to define the position and orientation of the first radial section across the eddy center for the collection of *in situ* ADCP and CTD (or XBT in case of bad sea conditions) observations. The ADCP measurements collected by the ship hull-mounted ADCP were then used to identify the position of the eddy center after each ship transect based on the algorithm developed by Nencioli et al. (2008). In the case of Latex08, this was done post cruise. However, for Latex09, the data processing chain was optimized and the work was done on-board in near real-time. This way, the precision of the center position was greatly improved compared to that estimated qualitatively from satellite imagery. The sampling strategy of the rest of the campaign was adapted with respect to each new calculated eddy center position, with the deployment of SVP drifters at the center or the edge of the eddy and multiple transects crossing the center either orthogonally or in a "butterfly" trajectory (Fig. 6 and refer to Hu et al. (2011b); Kersalé et al. (2013) for details).

### 4.2 Direct LCS iterative sampling (Latex10 - *R/V Téthys II*)

In the absence of a marked mesoscale structure, instead of the planned tracking and tracer injection of an eddy, the strategy was adapted to a (sub)mesoscale process study. The complexity of features visible from satellite chlorophyll-a and pseudo-SST maps, model circulation outputs and glider data rendered this task particularly challenging. The process study included the direct real-time detection of LCSs. This was tested with a novel, iterative, *in situ* sampling

1 strategy (Nencioli et al., 2011) which combined satellite altimetry data, ship-  
 2 based ADCP measurements, and iterative Lagrangian drifter releases (Fig-  
 3 ure 7). Three arrays of drifters were released at intervals of a few days to  
 4 obtain *in situ* estimates of the structures. The dispersion pattern of the first  
 5 drifter array on September 12 confirmed the presence of the along-shelf LCSs  
 6 associated with the NC identified from AVISO velocities (Figure 7a). The de-  
 7 ployment position and the spatial configuration of the second and third array  
 8 were chosen on the basis of the outcome of the previous launches. *In situ* re-  
 9 pelling (red) and attracting (blue) LCSs identified and tracked the migration of  
 10 an hyperbolic point for a period of 12 days, indicating that Lagrangian diagnos-  
 11 tics such as FTLE and FSLE can be successfully identified even in the complex  
 12 and variable flows typical of coastal regions (Nencioli et al., 2011). Neverthe-  
 13 less, *in situ*-based LCSs (also confirmed by ADCP observations) showed an  
 14 opposite circulation compared to the AVISO field over the continental shelf,  
 15 confirming the limitation of traditional altimetry for reliable transport anal-  
 16 ysis in those regions (Nencioli et al., 2011). To develop methods to mitigate  
 17 such altimetry limitations in coastal environment, LATEX float trajectories  
 18 were used to test the use of region-specific optimal interpolation methods to  
 19 generate maps of satellite-derived geostrophic current anomalies, ultimately  
 20 providing better absolute geostrophic currents, once added to different mean  
 21 circulation fields (Bouffard et al., 2014). Otherwise, during the cruise, the iden-  
 22 tification of the LCSs contributed to accurately identifying the location of the  
 23 thermal front described in Section 3 and tracking its evolution, particularly  
 24 when satellite imagery of pseudo-SST and ocean colour was not available due  
 25 to cloud cover. This provided a decisive contribution for i) optimizing the sam-  
 26 pling strategy for the collection of cross-front sections (Section 5.1), and ii)  
 27 tracking the movement of water masses for the quantification of the cross-shelf  
 28 fluxes associated with the front (Section 5.2).

#### 29 4.3 Tracer release (Latex00 - *R/V Téthys II*, and Latex10 - *R/V Le Suroît*)

30 One of the goals of the Latex10 field experiment was to mark a dynamical  
 31 mesoscale feature by releasing a passive tracer together with an array of La-  
 32 grangian buoys. The goal was to release the tracer in an initial patch as homo-  
 33 geneous as possible in the horizontal, and to study its turbulent mixing and  
 34 dispersion while minimizing the contribution due to the advection. For that,  
 35 it was necessary to continuously adjust the vessel route in order to remain as  
 36 closely as possible in the Lagrangian reference frame moving with the inves-  
 37 tigated mesoscale structure. To accomplish this task, two of the four LATEX  
 38 field campaigns were dedicated to the development of such a methodology.  
 39 The first campaign, Latex00, aimed at demonstrating its feasibility; the last  
 40 one, Latex10, performed a final test followed by the actual tracer experiment.

41 To perform the initial tracer release and subsequent mappings in a La-  
 42 grangian reference frame, the movement of the targeted water mass was tracked  
 43 using a reference buoy as a proxy. Our approach consisted in solving a classical

1 ballistic problem to obtain, in real-time and in a moving water mass, the direc-  
2 tion and distance to the next turn point of a chosen geometric route (details  
3 in Doglioli et al. (2013)). Results from the two field experiments showed that  
4 accuracy and frequency of acquisition of both vessel and buoy positions are  
5 key aspects for the successful implementation of this methodology.

6 The observational experience and analytical tools developed within LATEX  
7 led to a successful Lagrangian tracer release during the Latex10 experiment.  
8 The area for the tracer dispersion experiment was selected combining the nu-  
9 merical model results with those from the near real-time analysis of FSLEs  
10 computed from satellite-altimetry derived currents (Nencioli et al., 2011). The  
11 tracer was released in a patch of dimensions roughly  $25 \text{ km}^2 \times 25 \text{ m}$ , smaller  
12 than initially planned. After the release, the horizontal evolution of the tracer  
13 patch was monitored for 7 days during a series of 4 successive horizontal map-  
14 pings done at 7 m depth, the depth of the tracer release (Kersalé et al., 2015).

15 The software developed for the Lagrangian tracer experiment is included  
16 in the LATEXtools software suite. Our methodology presents some important  
17 technological improvements with respect to previous tracer studies related to  
18 both the positioning of the central buoy and the communication system with  
19 it. The software is also equipped with a series of graphical and user-friendly  
20 accessories. LATEXtools is written in Matlab, and can be freely downloaded  
21 from [www.mio.univ-amu.fr/LATEX](http://www.mio.univ-amu.fr/LATEX).

## 22 5 Horizontal mixing and cross-shelf exchanges

23 The tracer experiment from the *R/V Le Suroît* during Latex10 allowed a first  
24 estimate of lateral diffusivity at (sub)mesoscale (Kersalé et al., 2015). A second  
25 estimate was obtained by combining the strain rate from the drifter release,  
26 with the temperature and salinity gradients from thermosalinograph observa-  
27 tions collected aboard the *R/V Thélys II* (Nencioli et al., 2013). Finally, the  
28 combined analysis of *in situ* measurements and numerical modeling results  
29 provided a quantification of surface cross-shelf fluxes in the western GoL, the  
30 ultimate goal of the LATEX project.

### 31 5.1 Lateral diffusivities from tracer release and cross-front transects

32 The dispersion of the patch of the passive tracer  $SF_6$ , released in the adaptive  
33 Lagrangian framework described in 4.3, was used to obtain a first estimate of  
34 the lateral diffusivity in the coastal waters of the western part of the GoL.  
35 After having quantified atmospheric loss of the  $SF_6$ , the temporal evolution of  
36 the patch was fit with a diffusion-strain model to obtain estimates of the strain  
37 rate  $\gamma=2.5 \cdot 10^{-6} \text{ s}^{-1}$  and of the lateral diffusivity coefficient  $K_h=23.2 \text{ m}^2 \text{ s}^{-1}$   
38 (Fig. 8, top panel). To test the robustness of this estimate, a steady state model  
39 was also applied, showing  $K_h$  values similar to the diffusion-strain model after  
40 a period of adjustment between 2 and 4.5 days. This implied that, after such

1 period, the computation of  $K_h$  became independent from the further straining  
 2 of the patch. The thermal front present southeast of the initial patch clearly  
 3 affected the dynamics within the region and thus the temporal evolution of  
 4 the patch (see Kersalé et al. (2015) for additional details). Nonetheless the re-  
 5 sults were consistent with previous studies in the open ocean (refer to the end  
 6 of the section for more details) and demonstrated the success and feasibility  
 7 of these methods also under small-scale, rapidly-evolving dynamics typical of  
 8 coastal environments. However, one should note that this type of approach is  
 9 still a challenge. Among the difficulties encountered, some are worth mention-  
 10 ing: issues related to fitting a Gaussian dispersion model to a patch which,  
 11 under the stretching induced by the front, does not exhibit a Gaussian shape;  
 12 technical limitations, making it difficult to sample the whole fast-dispersing  
 13 patch, due both to vessel speed and  $SF_6$  analysis time, affecting the sampling  
 14 frequency. One of the objectives of the tracer experiment was also to deter-  
 15 mine the vertical diffusivity  $K_z$ , and to compare it with the values derived from  
 16 turbulence profiles acquired with the SCAMP. But lack of resolution in the  
 17 vertical sampling of the tracer made the imprecision of the method too large  
 18 to obtain reliable estimates. Nonetheless, turbulence profiles, acquired with  
 19 the SCAMP, have been used in a numerical study investigating the impact of  
 20 turbulence closure schemes and boundary conditions on the evaluation of  $K_z$   
 21 and energy dissipation rate (Costa et al., 2016).

22  
 23 A second estimate of *in situ* lateral diffusivity coefficients at the (sub)mesoscale  
 24 was based on an analogous hypothesis of balance between mesoscale straining  
 25 and small scale mixing adopted for passive tracer experiments. However, in-  
 26 stead of using the shape of the tracer patch, the analysis was based this time  
 27 on the width of the thermohaline front (Nencioli et al., 2013). The assump-  
 28 tion at the base of this second approach is that, once a near steady-state is  
 29 reached, the shape of the front will result from the balance between its strain-  
 30 induced steepening and its diffusion-induced relaxation. Such an approach has  
 31 already been applied by Flament et al. (1985), who quantified eddy diffusiv-  
 32 ity by combining the cross-front width derived from temperature variations  
 33 observed along a single ship-based cross-front section, with an approximate  
 34 estimate of the cross-front convergence rate derived from successive satellite  
 35 imagery of surface temperature. During Latex10, a series of front widths were  
 36 obtained, instead, by fitting multiple high-resolution temperature and salin-  
 37 ity cross-front sections with an analytical model for the cross-front profile at  
 38 the equilibrium. The front widths were then combined to the local strain rate  
 39 estimates derived from the dispersion of two arrays of Lagrangian drifters to  
 40 retrieve horizontal eddy diffusivities (see Nencioli et al. (2013) for details on  
 41 the equations). Latex10 adaptive sampling allowed the collection of 19 cross-  
 42 front transects within a span of 9 days, from which a total of 76 estimates of  
 43 lateral diffusivity  $K_h$  (19 SST transects, 19 SSS transects and 2 estimates of  
 44 strain rate) were computed. Their distribution is log-normal with a broad peak  
 45 at values below  $2.5 \text{ m}^2 \text{ s}^{-1}$ , and by a relatively long tail of episodic occurrences  
 46 at values above  $7.5 \text{ m}^2 \text{ s}^{-1}$  (Fig. 8, bottom panel). The distribution ranged

1 from a lowest value of  $0.06 \text{ m}^2 \text{ s}^{-1}$  to a maximum value of  $46.67 \text{ m}^2 \text{ s}^{-1}$ , with  
2 70% of the values between  $0.4$  and  $5 \text{ m}^2 \text{ s}^{-1}$ . The mean  $K_h$  computed using  
3 all estimates available was  $3.98 \text{ m}^2 \text{ s}^{-1}$ , with a standard deviation of  $7.26$   
4  $\text{m}^2 \text{ s}^{-1}$ . Further details on  $K_h$  statistics, including the impact of higher but  
5 less frequent estimates, can be found in (Nencioli et al., 2013). Despite some  
6 expected differences, the distribution of  $K_h$  estimated from the SST profiles  
7 was characterized by a similar shape as the one from the SSS profiles (Fig. 8,  
8 bottom panel). Moreover it is noteworthy that, although being characterized  
9 by different ranges, SST and SSS gradients from the same section returned  
10 similar estimates of  $K_h$ . This was an important feature since it showed that  
11 the estimates of  $K_h$  using this approach were primarily controlled by the front  
12 width and were, at the same time, relatively independent from the magnitude  
13 of the tracer variation across the front.

14 The mean values of  $K_h$  obtained with the two methods corresponded, re-  
15 spectively, to spatial scales of the order of i) the width of the patch (10 km) or  
16 ii) the cross-front distance (here below 5 km). As mentioned in the introduc-  
17 tion, at scales on the order of  $10 \text{ km}$ , lateral diffusivities had been found of the  
18 order of  $10 \text{ m}^2 \text{ s}^{-1}$  (Ledwell and Watson, 1991; Holtermann et al., 2012). These  
19 results are also in agreement with the estimates from the LatMix project in  
20 summer 2011, a year after Latex10. LatMix used different tracers (rhodamine  
21 and fluorescein) and mapping techniques (lidar) than LATEX. Isopycnal dif-  
22 fusivities were also calculated from drifter trajectories. The values obtained  
23 were of the order of  $1 \text{ m}^2 \text{ s}^{-1}$  at scales on the order of 1-5 km (Shcherbina  
24 et al., 2015).

## 25 5.2 Surface cross-shelf fluxes

26 During the LATEX project, two main dynamical situations were observed in  
27 the western part of the GoL:

- 28 1. the presence of an anticyclonic eddy, during which exchanges were investi-  
29 gated from a numerical model, backed-up by Latex09 observations;
- 30 2. the case of a frontal structure when no eddy was present; the exchanges  
31 were quantified from Latex10 observations.

32 When a mesoscale structure is present in the western part of the GoL, it can  
33 lose a portion of itself by a peeling mechanism either linked to the topography  
34 (Nof, 1999) or to the large scale forcing (for example, squeezing by the NC such  
35 as in Kersalé et al. (2013), previously described in section 3). These detached  
36 bits are generally transient structures, that can move relatively quickly out of  
37 the Gulf, contributing to the cross-shelf exchanges. In 2009, two Lagrangian  
38 floats, deployed in the LatexA2.09 eddy, rotated in it for, respectively, two  
39 and four and a half days (Fig. 9). The float that had stayed the longest in the  
40 eddy was then caught in the coastal northward jet. The other one left the eddy  
41 and moved southward performing anticyclonic rotations. These, although in  
42 the clockwise direction, were not due to inertial oscillations, since their period

1 was about 39 hours (while the near-inertial oscillations (NIO) have a period  
2 of 17.5 hours). The numerical simulations provided the necessary information  
3 to explain such drifter trajectory. Fig. 9 shows the drifters trajectories su-  
4 perposed to modeled relative vorticity, suggesting that the southward moving  
5 drifter joined another eddy present in the Catalan basin. The position of the  
6 Catalan eddy is located in the model further east than suggested by the float  
7 rotations. Despite the use of hybrid sigma coordinates, the strong bathymetry  
8 gradients are probably responsible for this shift in modeled circulation fea-  
9 tures. Nevertheless, the numerical simulations confirmed the mass exchanges  
10 modulated by eddy activity between the GoL and the Catalan shelf. The mass  
11 of the transient structure represented a third of the initial LatexA2\_09 eddy  
12 mass. The latter lost  $\sim 40\%$  of its mass during the separation. The mass (or  
13 volume) contribution to the Catalan eddy could not be assessed, the latter  
14 being cut by the model boundary. The volume of the transient structure is  
15 estimated to  $12.1 \pm 0.1 \text{ km}^3$ . This flux leaving the GoL could occur several  
16 times during the life of an eddy.

17 When no mesoscale eddies are present, the outer edge of the western GoL  
18 is characterized by the thermal front observed during Latex10 (see Section 3).  
19 The analysis integrated the observations from multiple platforms in order to:  
20 i) identify the different water masses, their origins and track their movements;  
21 ii) remove the signal associated with NIO from instantaneous ADCP veloci-  
22 ties; and hence iii) calculate accurate cross-shelf exchanges within the upper  
23 mixed layer associated with the front (Nencioli et al., 2016). Water masses  
24 were identified and tracked from successive satellite imagery and Lagrangian  
25 observations (see Section 2.3). The reconstructed *in situ* LCSs also provided  
26 a reference frame to quantify cross-shelf exchanges. Since the flow associated  
27 with the front was approximately nondivergent, the transport of a given water  
28 volume along the LCS tangle was conserved for different sections across the  
29 structures. Therefore, sections across the LCSs were used to compute cross-  
30 shelf exchanges even if not collected along the GoL boundary (i.e. the continen-  
31 tal slope). Finally, Lagrangian drifter trajectories were also used to quantify  
32 NIO. Strong NIO can have important impacts on current strengths and fluxes  
33 in the region (Millot and Crépon, 1981; Petrenko et al., 2005, 2008). Most of  
34 the Latex10 drifter trajectories exhibited several clockwise loops with period  
35 around  $\sim 17.5$  hours, indicating the presence of NIO. The time-series of their  
36 zonal and meridional components evidenced large oscillations superimposed  
37 to a slowly varying mean. As expected, the two components were out of phase  
38 by  $90^\circ$ , with positive meridional components preceding positive zonal ones.  
39 Following Haza et al. (2008), the mean velocity components were retrieved by  
40 applying a moving average based on a Gaussian window with a full width at  
41 half maximum (FWHM) of 17.5 hours. The NIO components were then com-  
42 puted as the residuals, i.e. the difference between original and averaged values.  
43 These NIO components were removed from the instantaneous ADCP observa-  
44 tions from the cross-front sections used to compute the cross-shelf exchanges.  
45 Limits of integration along each section were defined based on thermosalino-

graph observations which were used to identify the boundaries between the various outflowing and inflowing water masses.

The results indicated an average outflow of  $0.074 \pm 0.012$  Sv and an inflow of  $0.021 \pm 0.006$  Sv (Fig. 10). Integrated over the two-week lifetime of the front, such outflow would induce a total export of  $\sim 90 \pm 14$  km<sup>3</sup> of water. Thus, 3 to 4 of such events would be sufficient to completely renew the surface waters of the GoL. The total water import amounted to only  $\sim 25 \pm 7$  km<sup>3</sup>, less than a third of the outflow, hence suggesting larger inflows at depth or in the eastern part of the gulf to maintain the GoL volume balance. These *in situ* estimates represent a key term of comparison for the further development of numerical model- and satellite-based studies of cross-shelf exchanges associated with this type of processes. These cross-shelf exchanges can have impacts on biogeochemistry and ecology, as they can regulate the fluxes of carbon (Bauer and Druffel, 1998; Gattuso et al., 1998) and nutrients (Grantham et al., 2004), as well as the dispersion of fish-larvae (Roughan et al., 2006) and pollutants (Gustafsson et al., 1998).

## 6 Conclusion

The results of the physics component of the LATEX project have addressed the three main questions raised in Section 1.

1) Mesoscale dynamics in the western GoL includes coastal mesoscale eddies or strong fronts. The eddies are elliptic, baroclinic and anticyclonic. They are generated either by the combined effect of strong wind and stratification or by boundary current meanders (Hu et al., 2009, 2011b,a; Kersalé et al., 2013). The observed strong thermal (and saline) front was density-compensated (Nencioli et al., 2013). The front generation was mainly driven by the stirring induced by the interaction between wind-forced and large-scale circulation.

2) Field experiments were designed to investigate coastal (sub)mesoscale structures. Throughout a series of successive oceanographic cruises, LATEX developed and optimized a methodology for an adaptive Lagrangian sampling. Such adaptive approach was successfully applied to detect coastal eddies (Hu et al., 2011b; Kersalé et al., 2013), to identify Lagrangian Coherent Structures (Nencioli et al., 2011), and used for the initial release of a passive tracer as homogeneously as possible in a Lagrangian framework (Doglioli et al., 2013).

3) Horizontal mixing and cross-shelf exchanges were quantified. Lateral diffusivity coefficients, calculated using different approaches, are in the range classically encountered for their associated scales (Kersalé et al., 2015; Nencioli et al., 2013). To calculate  $K_h$ , the project included both a more traditional passive tracer experiment, as well as a novel technique based on the combined analysis of strain rate and thermohaline gradients. The strain rate was obtained from the analysis of the Lyapunov exponents derived from the La-

1 grangian floats (Nencioli et al., 2013).

2 Cross-shelf exchanges are strongly influenced by the dynamical conditions at  
3 the shelf edge. In the western GoL, these can be characterized by the pres-  
4 ence of either mesoscale eddies or strong thermohaline fronts. Eddies can trap  
5 waters in their core (Hu et al., 2011a) but can also get eroded by the slope  
6 current, losing non negligible percentage of their mass (Kersalé et al., 2013) all  
7 the way to potentially disappearing in the process. Fronts can act like corri-  
8 dors favoring strong cross-shelf inter-regional exchanges (Nencioli et al., 2016).

9  
10 This paper has summarized the (sub)mesoscale dynamics studied during  
11 LATEX. Since all LATEX field experiments occurred in late summer, the focus  
12 has been mainly on stratified conditions. A schematic of the main surface cir-  
13 culation processes that can occur in the western GoL can be found in Fig. 11.  
14 This schematic of the surface layer exhibits four main dynamical conditions: a)  
15 retention of water by an eddy; b) peeling of an eddy into a transient structure  
16 and GoL-exiting cross-shelf flux at the southern edge; c) frontal structure and  
17 associated southward fluxes, as during Latex10; d) intrusion of a barotropic  
18 current on the shelf between the coast and the NC, during Northwestern wind.  
19 The first three cases were encountered during LATEX. The last case was stud-  
20 ied numerically but with scarce *in situ* data collected before LATEX (Petrenko  
21 et al., 2008).

## 22 7 Perspectives

23 The arrival of the US-French wide-swath altimetry mission SWOT (Surface  
24 Water Ocean Topography, scheduled for 2021) will also be welcomed to im-  
25 prove the accuracy of the representation of coastal circulation structures and  
26 their temporal evolution. Thanks to its Synthetic Aperture Radar (SAR) in-  
27 terferometer, the SWOT satellite will provide precise altimetry measurements  
28 close to the coast. SWOT will also increase by an order of magnitude the  
29 resolution of 2D maps of sea surface height (SSH). As shown by LATEX mod-  
30 eling and *in situ* activities, coastal eddies and fronts have an important role  
31 in modulating cross-shelf exchanges, but due to their potentially small size  
32 they are often invisible in SSH images. Therefore, these structures are often  
33 detected only indirectly, either by *in situ* techniques - like drifter or glider  
34 experiments - or through remote sensing, by their signature in SST or Chl  
35 images. The availability of SWOT data will mark a new generation of exper-  
36 iments because it will relieve *in situ* operations from the task of identifying  
37 and following in time the fine-scale physical features. Once these features are  
38 accessible from remote sensing, *in situ* experiments will have the possibility  
39 of concentrating on the characterization of the fine-scale dynamics, using im-  
40 ages of high-resolution altimetry for tracking submesoscale features, such as  
41 filaments and small eddies. This way, ship-time will be fully available for a  
42 proper characterization of the 3D dynamics occurring in between the meso-  
43 and the submeso-scale, addressing key uncertainties like the quantification of

1 vertical fluxes of nutrient and carbon in frontal systems. In this regard, the  
2 Mediterranean sea is set to play a special role: due to its easy accessibility,  
3 small Rossby radius, energetic boundary currents, very low cloud coverage,  
4 and low tides, it is an ideal 'pocket ocean' where to combine high-resolution  
5 satellite observations and multi-platform *in situ* experiments. SWOT is ex-  
6 pected to resolve features down to 15 km including near the coast. In turn,  
7 this information will hopefully improve the realism of circulation models, in  
8 particular their representation of biogeochemical processes.

9 This Review concentrated on the physics component of LATEX. So only  
10 a short summary is given here on what has been done concerning physical-  
11 biogeochemical coupling and the perspectives that this work opens. The LA-  
12 TEX numerical study of the GoL circulation has allowed for the quantifica-  
13 tion of the impact of the anticyclonic eddy A1\_01 on the ecosystem dynamics  
14 (Campbell et al., 2013). Additionally, the circulation model Symphonie was  
15 coupled with a biogeochemical model originating from the Eco3M modeling  
16 platform (Baklouti et al., 2006a,b), and adapted as a pelagic plankton ecosys-  
17 tem model for the Northwestern Mediterranean basin by Auger et al. (2011).  
18 The eddy exhibited low productivity at its core and rising up of nutricline  
19 on its edges. However the functioning and consequences of the coastal eddy  
20 on nutrients and plankton distributions was complicated by potential interac-  
21 tions with topography, wind-induced upwelling along the coast and the nearby  
22 Northern Current. This coupled modeling is to be pursued to compare the nu-  
23 merical results with the *in situ* data collected during the Latex cruises (F. Diaz,  
24 LATEX PI for biogeochemistry; pers. comm.). More work needs to be done  
25 in order to estimate not only the impacts of LATEX eddies on biogeochemi-  
26 cal budgets and cross-shelf transfers, but also to comprehend the coupling of  
27 physics and biogeochemistry at (sub)mesoscale in this zone.

28 The LATEX adaptive real-time Lagrangian strategy needs also to be ac-  
29 companied with 3D *in situ* observations and fast, automated physical and  
30 biogeochemical sampling in order, among others, to explore surface semi-  
31 geostrophic model (Badin, 2013) and to study processes associated with ed-  
32 dies, fronts and filaments (e.g. frontogenesis/frontolysis as in Hoskins (1982)),  
33 as well as coupled physical-biogeochemical processes at the submesoscale. This  
34 challenge was already highlighted in the open ocean (Lévy et al., 2012), and  
35 remains highly relevant in the coastal environment.

### 36 Availability of the LATEX and SPASSO codes

37 The LATEXtools software (Doglioli et al., 2013) is available freely on the  
38 LATEX web site: [www.mio.univ-amu.fr/LATEX](http://www.mio.univ-amu.fr/LATEX). To our knowledge, no other  
39 papers report detailed descriptions of the techniques and software adopted  
40 for Lagrangian tracer release and sampling strategy, although they are a key  
41 point for the success of *in situ* tracer experiments. We are nonetheless aware  
42 of the now available Google Earth interactive map of the LatMix project  
43 (<http://dx.doi.org/10.1175/BAMS-D-14-00015.2>). Since 2010, the LATEX La-

1 grangian strategy has been further developed and successfully applied during  
2 several other ocean campaigns such as KEOPS2 in 2011 (Quéguiner, 2011;  
3 d’Ovidio et al., 2015), STRASSE in 2012 (Reverdin et al., 2015) and, in  
4 2015, OUTPACE (Moutin and Bonnet, 2015) and OSCAHR (Doglioli, 2015).  
5 In the continuity of LATEXtools, SPASSO (Software Package for an Adap-  
6 tive Satellite-based Sampling for Ocean campaigns, available at [www.mio.  
7 univ-amu.fr/SPASSO](http://www.mio.univ-amu.fr/SPASSO)) retrieves and processes satellite data on land and then  
8 transmits them on board. The analysis of the collected information (including  
9 *in situ* data and available model predictions, in addition to the satellite data) is  
10 done on land and allows to prepare daily bulletins with suggestions for optimal  
11 ship routing and station positioning. These bulletins are then send on board,  
12 as well as made available through dedicated web pages. SPASSO is planned to  
13 be used for the cruises PEACETIME (2017, PIs: C. Guieu and K. Desboeufs),  
14 SARGASSES (2017, PIs: L. Berline and T. Thibaut) and BIOSWOT (2018,  
15 PI: F. d’Ovidio).

16 **Acknowledgements** The LATEX project was supported by the programs LEFE/IDAO  
17 and LEFE/CYBER of the INSU-Institut National des Sciences de l’Univers and by the  
18 Region PACA-Provence Alpes Côte d’Azur. The PIs of the project were A. Petrenko for  
19 the physics component and F. Diaz for the biogeochemical component. The chief scientists  
20 were A. Petrenko on board the *R/V Téthys II* for Latex00, Latex07, Latex08, Latex09  
21 and Latex10 and B. Quéguiner on board the *R/V Le Suroît* for Latex10. The scientist  
22 in charge of the tracer release was S. Blain. M. Kersalé and Z.Y. Hu were financed by  
23 MENRT Ph.D. grants. F.Nencioli acknowledges support from the FP7 Marie Curie Actions  
24 of the European Commission, via the Intra-European Fellowship (FP7-PEOPLE-IEF-2011),  
25 project “Lyapunov Analysis in the COaSTal Environment” (LACOSTE-299834). We thank  
26 I. Dekeyser for his support and useful discussions. We have appreciated that Claude Es-  
27 tournel and Patrick Marsaleix provided us the initial Symphonie code and helped us along  
28 our configuration development. We acknowledge the MFSTEP program for OGCM outputs.  
29 Meteorological and AVHRR data were supplied by Météo-France. The DT-INSU is thanked  
30 for the treatment of the thermosalinograph data. The altimeter products were produced  
31 by Ssalto/Duacs and distributed by Aviso with support from CNES, that also financed the  
32 post-doc fellowship of Jérôme Bouffard. The MODIS Aqua data were supplied by the Dis-  
33 tributed Active Archive Center at NASA Goddard Space Flight Center and made possible  
34 by the MODIS Project. We thank the crews and technicians of the *R/V Le Suroît* and the  
35 *R/V Téthys II*, the DT-INSU and all the LATEX collaborators for their assistance at sea or  
36 during the project. A special thanks goes to, in alphabetical order: Anne Desnues, Jean-Luc  
37 Fuda, Nicolas Grima, Thierry Labasque, Deny Malengros, Peggy Rimmelin, Gilles Rougier  
38 and Anna Roumyantseva, for their work on the data collection and Lagrangian strategy, as  
39 well as Emmanuel Bosc for some chlorophyll-a satellite products.

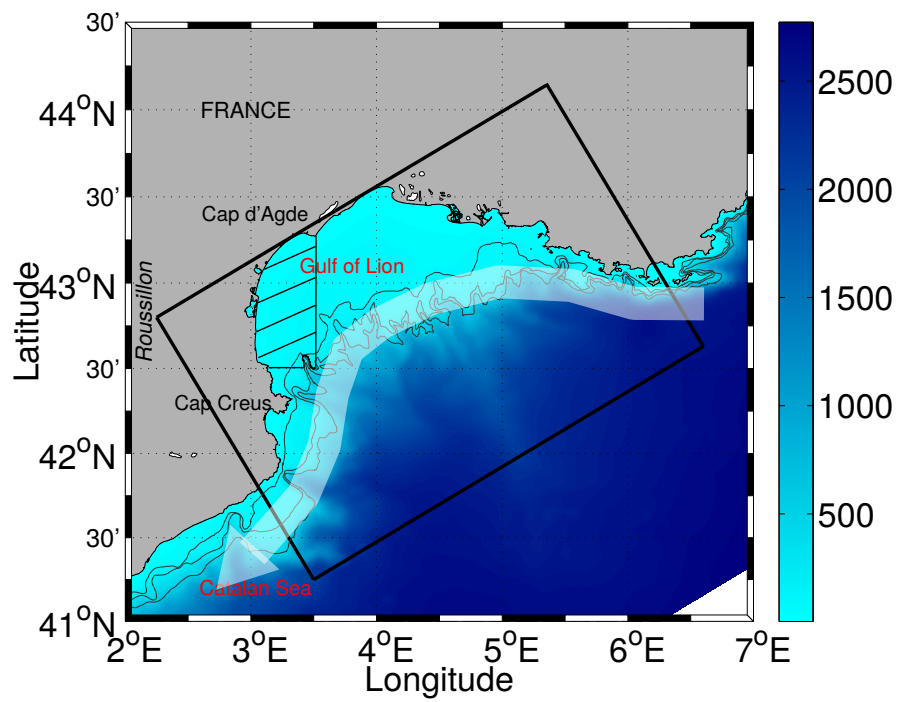


**Fig. 1** Bathymetry of the Gulf of Lion. The rectangle represents the 1 km resolution model domain. Shaded color represents the bathymetry [m]. Isobaths at 100, 200 and 500 m are plotted with thin lines. The white arrow shows the mean position of the Northern Current (NC). The hatched area indicates the zone where the absolute value of potential energy anomaly  $\phi$  is calculated

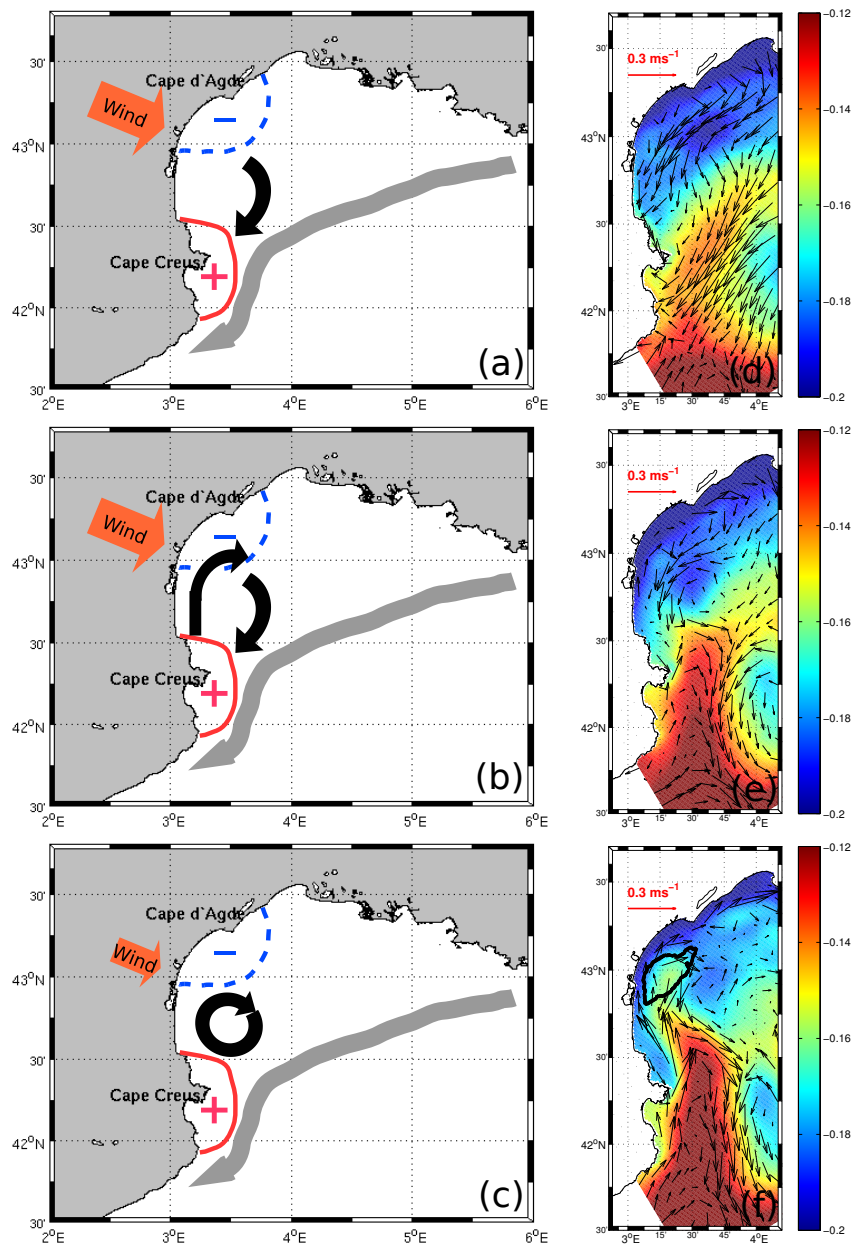


**Fig. 2** Schematic generation of an anticyclonic eddy (from the 8-year numerical study of (Hu et al., 2011b)). The three main phases of the eddy generation process are represented: a) upwelling and Ekman flow, b) generation of a northward coastal jet, c) eddy generation. Eddy-related currents are represented by black arrows; upwelling area, corresponding to a negative Sea Level Anomaly (SLA), designated by the blue dashes around the minus sign; positive SLA area around Cape Creus designated by the red area around the positive sign; wind represented by the orange arrow; the NC by the grey arrow along the continental shelf. As an example, corresponding modeled sea surface height and velocity field at 5 m depth on d) July 02, 2005; e) July 07, 2005; and f) July 10, 2005

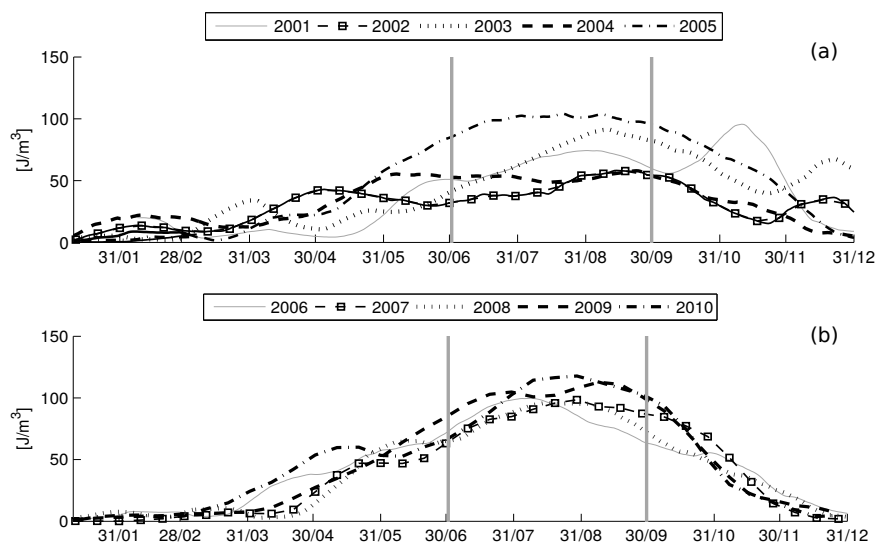


**Fig. 3** Time series of 30 day moving averaged potential energy anomaly [ $\text{Jm}^{-3}$ ] over the western part of the GoL for the upper 100 m depth for the years a) 2001 to 2005 and b) 2006 to 2010

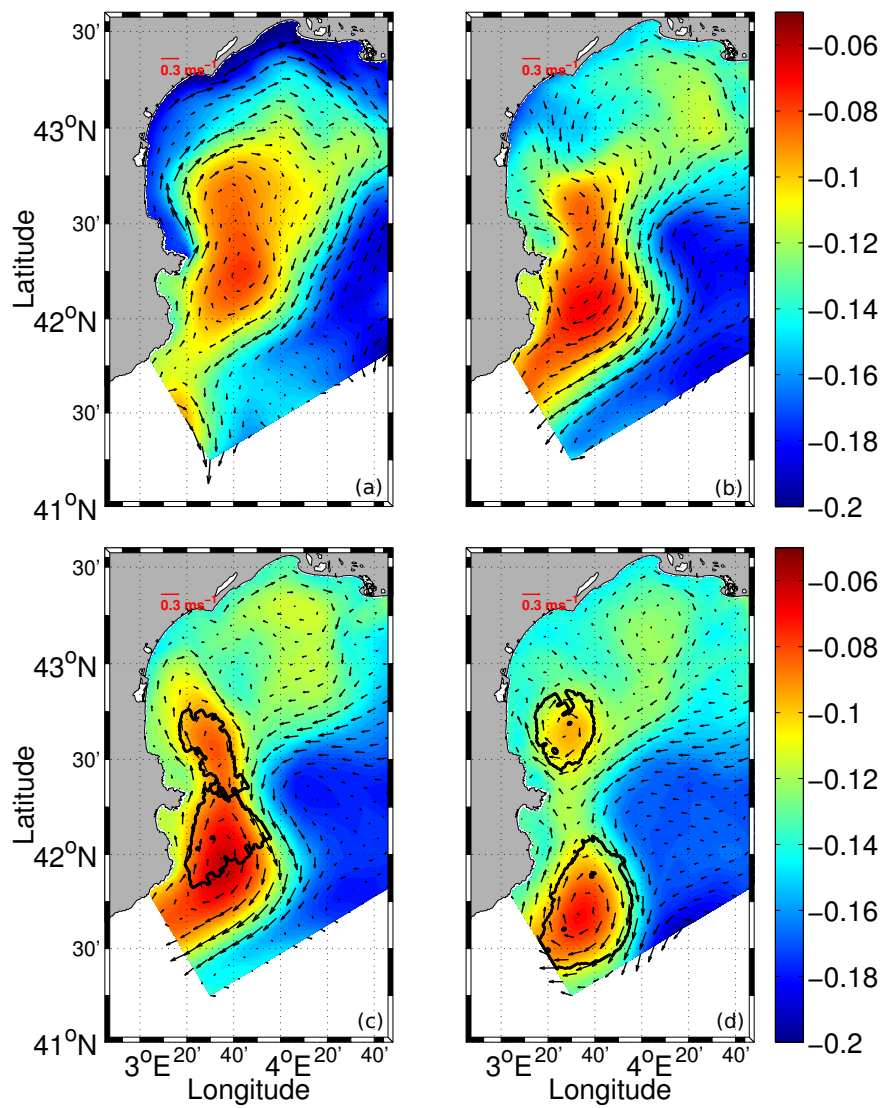


**Fig. 4** Temporal sequence of formation of the eddy, sea surface height [m] and velocity field at 5 m depth [ $\text{ms}^{-1}$ ], in four steps: July 20, Aug. 8, Aug. 16, and Aug. 27, 2009 (adapted from Kersalé et al. (2013), with permission)

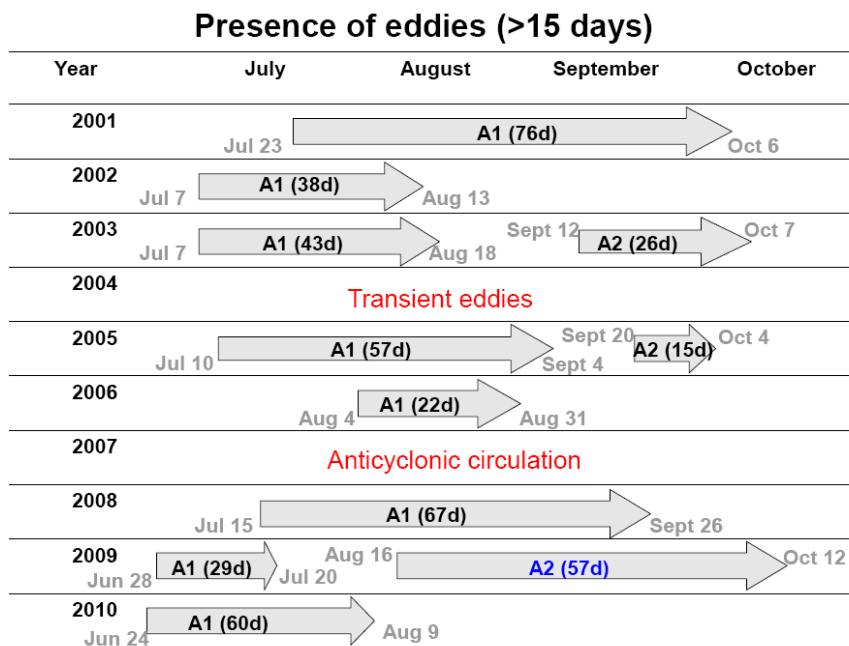


**Fig. 5** Gantt table of the long-life modeled eddies from 2001 to 2010. The grey arrows indicate the duration of the first A1 or second A2 eddies, with the corresponding number of days in parenthesis. When this is written in black, the eddy has been generated with the first generation process (Hu et al., 2011b). When in blue, it has been generated by the second generation process (Kersalé et al., 2013). The dates of birth and death of each eddy are also indicated

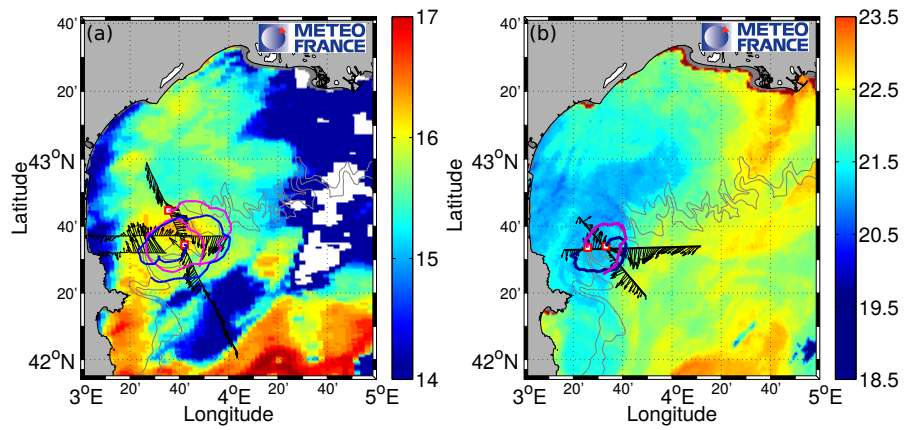


**Fig. 6** Eddies studied a) during Latex08, b) during Latex09. ADCP transects, with horizontal currents at 15 m depth in black. SVP drifter trajectories are shown in blue and purple during a) 6 days, b) 3 days following their release at the location indicated with a red square. Pseudo-SST images on a) Sept. 02, 2008 and b) Aug. 28, 2009.

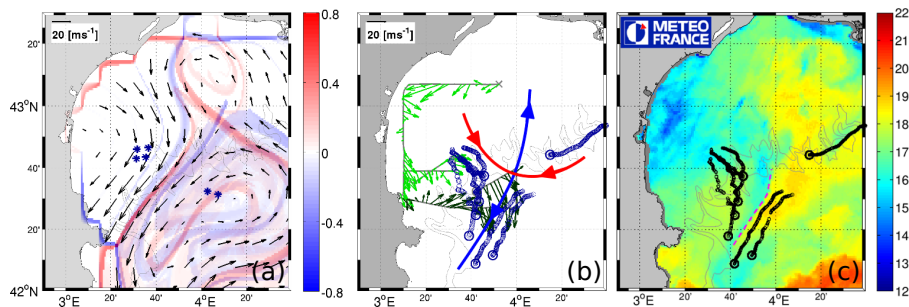


**Fig. 7** a) Lagrangian coherent structures, FSLE in  $[s^{-1}]$  derived from AVISO geostrophic velocities on 14 September 2010 and release position of the Lyap01 cluster of Lagrangian drifters. In blue are the attracting LCS (backward FSLE) and in red the repelling ones (forward FSLE). b) ADCP currents, 3-day drifter trajectories and position of the Lagrangian coherent structures reconstructed from *in situ* measurements. c) image of pseudo-SST for Sept. 14, 2010 and 3-day drifter trajectories. The position of the front focus of the Latex10 field experiment is marked by the magenta dashed line. (adapted from Nencioli et al. (2011, 2016) with permission)

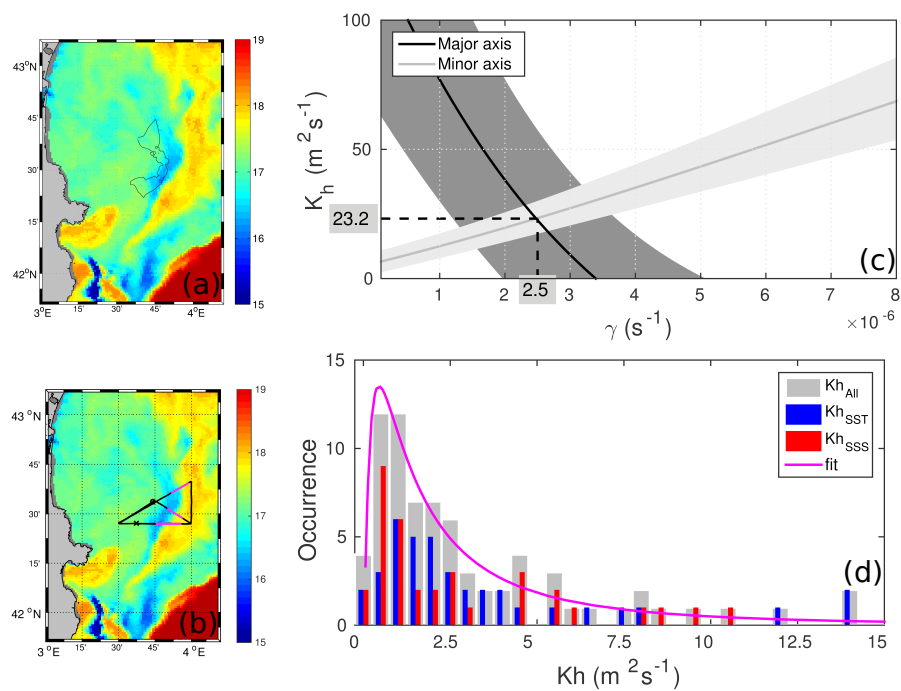


**Fig. 8** Spatial scales and diffusivity coefficients. a) Pseudo-SST map on Sept. 15, 2010 with the contour of the 3rd  $SF_6$  mapping; b) Same pseudo-SST map with examples of cross-front transects, the front SST gradient in red; c) The point of intersection of the two curves (major and minor axes, see Kersalé et al. (2015) for details) indicates the best estimates of  $\gamma$  [s<sup>-1</sup>] and  $K_h$  [m<sup>2</sup> s<sup>-1</sup>]. The shaded areas represent the uncertainties; d) Frequency histogram of the horizontal eddy diffusion coefficients derived by Nencioli et al. (2013). In blue is the distribution of the  $K_H$  estimated from the SST profiles only; in red the distribution of the  $K_H$  from the SSS profiles only; and in grey the total distribution of the two combined together

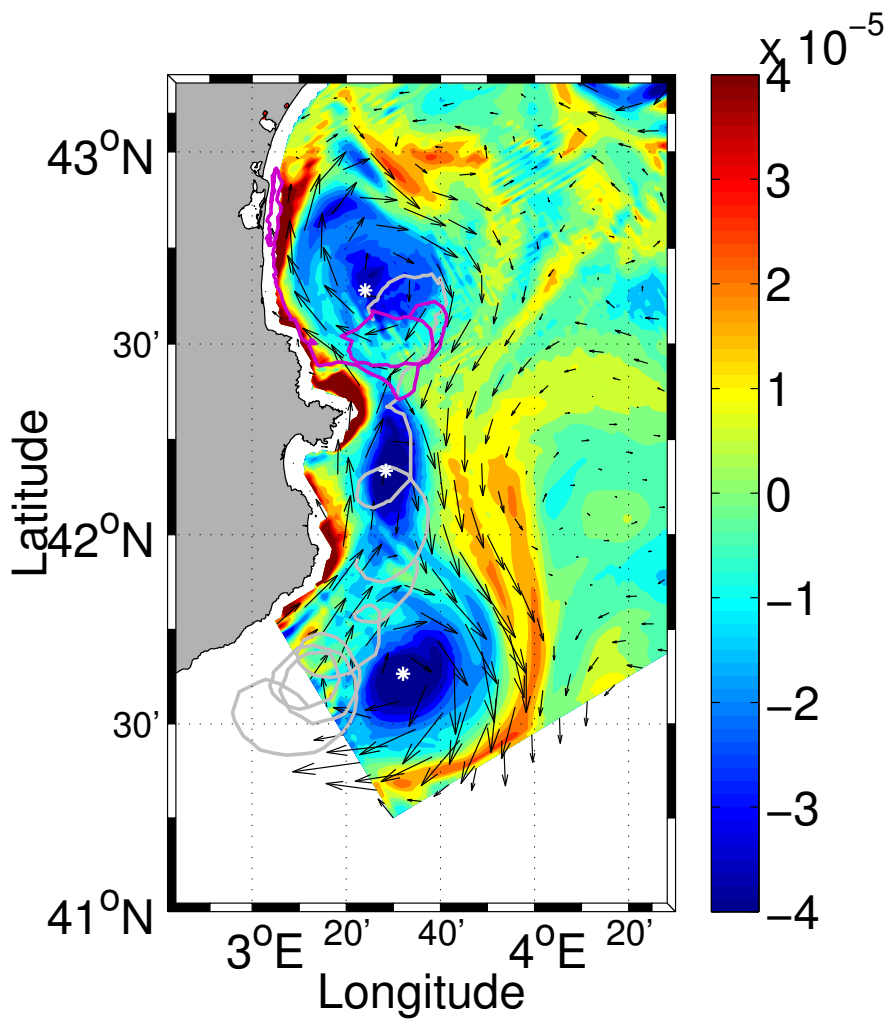


**Fig. 9** Transient structure detaching from LatexA2.09. Modeled relative vorticity [ $\text{s}^{-1}$ ], velocity field at 20 m depth on Sept. 3, 2009 (arrows) and drifter trajectories (grey and purple) from Aug. 26 to Sept. 11, 2009. The white stars represent each structure center

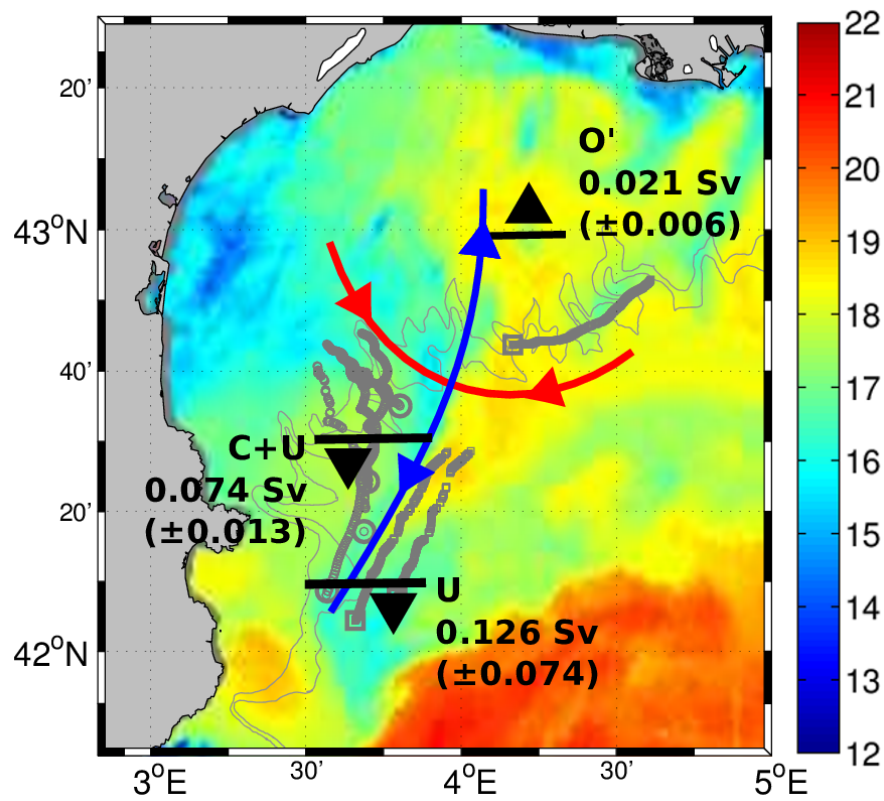


**Fig. 10** Schematics of the average cross-shelf fluxes associated with the front from Latex10, superimposed on pseudo-SST, buoy trajectories (grey) and in situ LCSs (red and blue). Locations of outflow and inflow of the U (upwelled), C (coastal) and O' (modified open, see Nencioli et al. (2016) for details) waters are indicated relative to the Lyap01 LCS, as no cloud-free pseudo-SST images are available afterwards. (adapted from Nencioli et al. (2016) with permission)

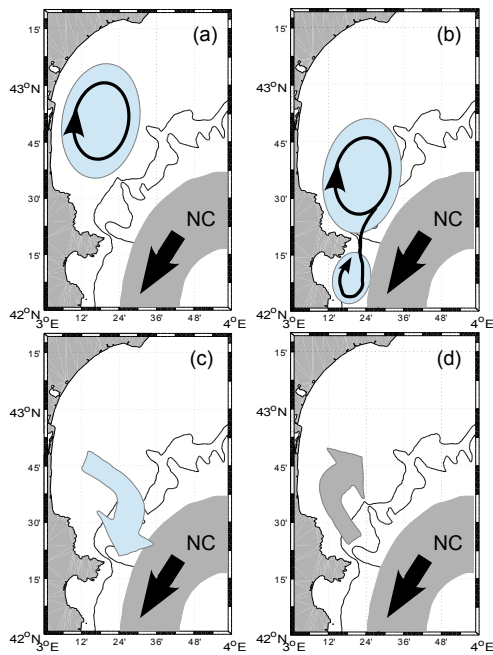


**Fig. 11** Schematic of 4 main circulation patterns in the western GoL; a) water eddy retention; b) transient feature leaking from eddy; c) cross-shelf flux exiting the GoL; d) coastal jet entering the GoL. Blue (grey) areas indicate the preferential zones of baroclinic (barotropic) circulation features

## References

- Abraham, E., Law, C., Boyd, P., Lavender, S., Maldonado, M., and Bowie, A. (2000). Importance of stirring in the development of an iron-fertilized phytoplankton bloom. *Nature*, 407:727–730.
- Allou, A., Forget, P., and Devenon, J. L. (2010). Submesoscale vortex structures at the entrance of the Gulf of Lions in the Northwestern Mediterranean Sea. *Cont. Shelf Res.*, 30:724–732.
- Auger, P. A., Diaz, F., Ulses, C., Estournel, C., Neveux, J., Joux, F., Pujo-Pay, M., and Naudin, J. J. (2011). Functioning of the planktonic ecosystem of the Rhone River plume (NW Mediterranean) during spring and its impact on the carbon export: a field data and 3-D modelling combined approach. *Biogeosciences*, 24(6):9039–9116.
- Aurell, E., Boffetta, G., Crisanti, A., Paladin, G., and Vulpiani, A. (1997). Predictability in the large: an extension of the concept of Lyapunov exponent. *J. Phys. A*, 30(1):1.
- Badin, G. (2013). Surface semi-geostrophic dynamics in the ocean. *Geophys. Astrophys. Fluid Dynam.*, 107(5):526–540.
- Baklouti, M., Diaz, F., Pinazo, C., Faure, V., and Quéguiner, B. (2006a). Investigation of mechanistic formulations depicting phytoplankton dynamics for models of marine pelagic ecosystems and description of a new model. *Prog. Oceanogr.*, 71(1):1–33.
- Baklouti, M., Faure, V., Pawlowski, L., and Sciandra, A. (2006b). Investigation and sensitivity analysis of a mechanistic phytoplankton model implemented in a new modular numerical tool (eco3m) dedicated to biogeochemical modelling. *Prog. Oceanogr.*, 71(1):34–58.
- Barrier, N., Petrenko, A. A., and Ourmières, Y. (2016). Strong intrusions of the Northern Mediterranean Current on the eastern Gulf of Lion: insights from in-situ observations and high resolution numerical modelling. *Ocean Dynam.*, 66(3):313–327.
- Bauer, J. E. and Druffel, E. R. M. (1998). Ocean margins as a significant source of organic matter to the deep open ocean. *Nature*, 392:482–485.
- Beron Vera, F. J., Olascoaga, M. J., and Goni, G. J. (2008). Oceanic mesoscale eddies as revealed by Lagrangian coherent structures. *Geophys. Res. Lett.*, 35(12).
- Biscaye, P. E. (1994). Shelf edge exchange processes in the southern middle atlantic bight: Seep-ii. *Deep Sea Res. I*, 41(2-3):229–230.
- Bosse, A., Testor, P., Houpert, L., Damien, P., Prieur, L., Hayes, D., Tailandier, V., Durrieu de Madron, X., d’Ortenzio, F., Coppola, L., Karstensen, J., and Mortier, L. (2016). Scales and dynamics of submesoscale coherent vortices formed by deep convection in the northwestern mediterranean sea. *J. Geophys. Res.*, 121(10):7716–7742.
- Bouffard, J., Nencioli, F., Escudier, R., Doglioli, A. M., Petrenko, A. A., Pascual, A., Poulain, P. M., and Elhmaidi, D. (2014). Lagrangian analysis of satellite-derived currents: Application to the North Western Mediterranean coastal dynamics. *Adv. Space Res.*, 53(5):788–801.

- 1 Bouffard, J., Vignudelli, S., Herrmann, M., Lyard, F., Marsaleix, P., Ménard,  
2 Y., and Cipollini, P. (2008). Comparison of ocean dynamics with a regional  
3 circulation model and improved altimetry in the North-western Mediter-  
4 ranean. In *Terr. Atmos. Ocean. Sci.*, volume 19, pages 117–133.
- 5 Brink, K. H. and Cowles, T. J. (1991). The Coastal Transition Zone program.  
6 *J. Geophys. Res.*, 96(C8):14637–14647.
- 7 Broche, P., Devenon, J.-L., Forget, P., de Maistre, J.-C., Naudin, J.-J., and  
8 Cauwet, G. (1998). Experimental study of the Rhone plume. Part I: physics  
9 and dynamics. *Oceanol. Acta*, 21(6):725–738.
- 10 Burchard, H. and Burchard, R. (2008). A dynamic equation for the poten-  
11 tial energy anomaly for analysing mixing and stratification in estuaries and  
12 coastal seas. *Estuar. Coast. Shelf S.*, 77(4):679–687.
- 13 Burchard, H., Craig, P. D., Gemmrich, J. R., van Haren, H., Mathieu, P.-P.,  
14 Meier, H. M., Smith, W. A. M. N., Prandke, H., Rippeth, T. P., Skillingstad,  
15 E. D., et al. (2008). Observational and numerical modeling methods for  
16 quantifying coastal ocean turbulence and mixing. *J. Phys. Oceanogr.*,  
17 76(4):399–442.
- 18 Campbell, R., F., D., Hu, Z., Doglioli, A., Petrenko, A., and Dekeyser, I.  
19 (2013). Nutrients and plankton spatial distributions induced by a coastal  
20 eddy in the Gulf of Lion. Insights from a numerical model. *Prog. Oceanogr.*,  
21 109:47–69.
- 22 Canals, M., Puig, P., de Madron, X. D., Heussner, S., Palanques, A., and  
23 Fabres, J. (2006). Flushing submarine canyons. *Nature*, 444(7117):354–7.
- 24 Capet, X., McWilliams, J., Molemaker, M., and Shchepetkin, A. (2008a).  
25 Mesoscale to submesoscale transition in the California Current System. Part  
26 I: Flow structure, eddy flux, and observational tests. *J. Phys. Oceanogr.*,  
27 38(1):29–43.
- 28 Capet, X., McWilliams, J. C., Molemaker, M. J., and Shchepetkin, A. (2008b).  
29 Mesoscale to submesoscale transition in the California Current System. Part  
30 II: Frontal processes. *J. Phys. Oceanogr.*, 38(1):44–64.
- 31 Costa, A., Doglioli, A., Marsaleix, P., and Petrenko, A. (2016). Comparison of  
32 in situ microstructure measurements to different turbulence closure schemes  
33 in a 3-D numerical ocean circulation model. *Ocean Model.*, (submitted).
- 34 Cotté, C., d’Ovidio, F., Chaigneau, A., Lévy, M., Taupier Letage, I., Mate,  
35 B., and Guinet, C. (2011). Scale-dependent interactions of Mediterranean  
36 whales with marine dynamics. *Limnol. Oceanogr.*, 106(20):219–232.
- 37 Crawford, W. R. (2002). Physical characteristics of Haida Eddies. *Journal of*  
38 *Oceanography*, 58(5):703–713.
- 39 Csanady, G. (1982). *Circulation in the coastal ocean*. D.Reidel Publishing  
40 Company, Kluwer Group, Dordrech, Holland.
- 41 Cushman-Roisin, B. (1994). *Introduction to Geophysical Fluid Dynamics*.  
42 Prentice Hall.
- 43 De Boer, G. J., Pietrzak, J. D., and Winterwerp, J. C. (2008). Using the po-  
44 tential energy anomaly equation to investigate tidal straining and advection  
45 of stratification in a region of freshwater influence. *Ocean Model.*, 22:1–11.

- 1 De Monte, S., D'Ovidio, F., Cotté, C., Lévy, M., Le Corre, M., and Weimer-  
2 skirch (2012). Frigatebird behaviour at the ocean-atmosphere interface:  
3 integrating animal behaviour with multisatellite data. *J. R. Soc. Interface*.
- 4 Di Lorenzo, E., Foreman, M. G. G., and Crawford, W. R. (2005). Modelling  
5 the generation of Haida Eddies. *Deep-Sea Res. II*, 52:853–873.
- 6 Doglioli, A. (2015). OSCAHR cruise, RV Téthys II,  
7 <http://dx.doi.org/10.17600/15008800>.
- 8 Doglioli, A., Nencioli, F., Petrenko, A. A., Fuda, J.-L., Rougier, G., and Grima,  
9 N. (2013). A software package and hardware tools for in situ experiments  
10 in a Lagrangian reference frame). *J. Atmos. Ocean. Tech.*, 30(8).
- 11 Doglioli, A. M., Blanke, B., Speich, S., and Lapeyre, G. (2007). Tracking coherent  
12 structures in a regional ocean model with wavelet analysis: application  
13 to Cape Basin Eddies. *J. Geophys. Res.*, 112.
- 14 d'Ovidio, F., De Monte, S., Alvain, S., Dandonneau, Y., and Lévy, M. (2010).  
15 Fluid dynamical niches of phytoplankton types. *Proc. Natl. Acad. Sci. U.*  
16 *S. A.*, 107(43):18366–18370.
- 17 d'Ovidio, F., Della Penna, A., Trull, T. W., Nencioli, F., Pujol, M.-I., Rio, M.-  
18 H., Park, Y.-H., Cotté, C., Zhou, M., and Blain, S. (2015). The biogeochem-  
19 ical structuring role of horizontal stirring: Lagrangian perspectives on iron  
20 delivery downstream of the Kerguelen Plateau. *Biogeosciences*, 12(19):5567–  
21 5581.
- 22 d'Ovidio, F., Fernández, V., Hernández-García, E., and López, C. (2004). Mix-  
23 ing structures in the mediterranean sea from finite-size lyapunov exponents.  
24 *Geophys. Res. Lett.*, 31:L17203.
- 25 Durrieu, de Madron, X., Houpert, L., Puig, P., Sanchez-Vidal, A., Testor,  
26 P., Bosse, A., Estournel, C., Somot, S., Bourrin, F., and Bouin, M. N.  
27 (2013). Interaction of dense shelf water cascading and open-sea convection  
28 in the northwestern mediterranean during winter 2012. *Geophys. Res. Lett.*,  
29 40(7):1379–1385.
- 30 Durrieu De, Madron, X., Zervakis, V., Theocharis, A., and Georgopoulos, D.  
31 (2005). Comments on "cascades of dense water around the world ocean".  
32 *Prog. Oceanogr.*, 64(1):83–90.
- 33 Estournel, C., Durrieu de Madron, X., Marsaleix, P., Auclair, F., Julliand,  
34 C., and Vehil, R. (2003). Observation and modeling of the winter coastal  
35 oceanic circulation in the Gulf of Lion under wind conditions influenced by  
36 the continental orography (FETCH experiment). *J. Geophys. Res.*, 108(C3).
- 37 Ferrari, R. (2011). A frontal challenge for climate models. *Science*,  
38 332(6027):316–7.
- 39 Flament, P., Armi, L., and Washburn, L. (1985). The evolving structure of an  
40 upwelling filament. *J. Geophys. Res.*, 90(C6):11765–11778.
- 41 Flexas, M. M., Durrieu de Madron, X., Garcia, M. A., Canals, M., and Arnau,  
42 P. (2002). Flow variability in the Gulf of Lions during the MATER HFF  
43 experiment (March-May 1997). *J. Mar. Sys.*, 33-34:197–214.
- 44 Garreau, P., Garnier, V., and Schaeffer, A. (2011). Eddy resolving modelling  
45 of the Gulf of Lions ans Catalan Sea. *Ocean Dynam.*, 61:991–1003.

- 1 Gaspar, P., Grégoris, Y., and Lefevre, J.-M. (1990). A simple eddy kinetic  
2 energy model for simulations of the oceanic vertical mixing: Tests at Station  
3 Papa and long-term upper ocean study site. *J. Geophys. Res.*, 95:179–193.
- 4 Gattuso, J.-P., Frankignoulle, M., and Wollast, R. (1998). Carbon and Car-  
5 bonate Metabolism in Coastal Aquatic Ecosystems. *Annu. Rev. Ecol. Syst.*,  
6 29:pp. 405–434.
- 7 Grantham, B. A., Chan, F., Nielsen, K. J., Fox, D. S., Barth, J. A., Huyer, A.,  
8 Lubchenco, J., and Menge, B. A. (2004). Upwelling-driven nearshore hy-  
9 poxia signals ecosystem and oceanographic changes in the northeast Pacific.  
10 *Nature*, 429:749–754.
- 11 Griffa, A., Kirwan, A., Mariano, A. J., Özgökmen, T., and Rossby, H. T.  
12 (2007). *Lagrangian Analysis and Prediction of Coastal and Ocean Dynamics*.  
13 Cambridge University Press.
- 14 Gustafsson, Ö., Buesseler, K. O., Geyer, W. R., Moran, S. B., and Gschwend,  
15 P. M. (1998). An assessment of the relative importance of horizontal and  
16 vertical transport of particle-reactive chemicals in the coastal ocean. *Cont.*  
17 *Shelf Res.*, 18(7):805–829.
- 18 Haller, G. (2011). A variational theory of hyperbolic Lagrangian Coherent  
19 Structures. *Physica D*, 240(7):574–598.
- 20 Haller, G. and Yuan, G. (2000). Lagrangian coherent structures and mixing  
21 in two-dimensional turbulence. *Physica D*, 147:352–370.
- 22 Haza, A. C., Özgökmen, T. M., Griffa, A., Molcard, A., Poulain, P.-M., and  
23 Peggion, G. (2010). Transport properties in small-scale coastal flows: rela-  
24 tive dispersion from VHF radar measurements in the Gulf of La Spezia.  
25 *Ocean Dyn.*, 60(4):861–882.
- 26 Haza, A. C., Poje, A. C., Özgökmen, T. M., and Martin, P. (2008). Rela-  
27 tive dispersion from a high-resolution coastal model of the Adriatic Sea.  
28 *Ocean Model.*, 22(1-2):48–65.
- 29 Holtermann, P. L., Umlauf, L., Tanhua, T., Schmale, O., Rehder, G., and  
30 Waniek, J. J. (2012). The Baltic Sea Tracer Release Experiment: 1. Mixing  
31 rates. *J. Geophys. Res.*, 117(C1).
- 32 Hopkins, J., Sharples, J., and Huthnance, J. M. (2012). On-shelf transport  
33 of slope water lenses within the seasonal pycnocline. *Geophys. Res. Lett.*,  
34 39(8):85–93.
- 35 Hoskins, B. (1982). The mathematical theory of frontogenesis.  
36 *Annu. Rev. Fluid Mech.*, 14:31–151.
- 37 Hu, Z. Y., Doglioli, A. M., Petrenko, A. A., Marsaleix, P., and Dekeyser, I.  
38 (2009). Numerical simulations of eddies in the Gulf of Lion. *Ocean Model.*,  
39 28(4):203 – 208.
- 40 Hu, Z. Y., Petrenko, A. A., Doglioli, A. M., and Dekeyser, I. (2011a). Nu-  
41 merical study of eddy generation in the western part of the Gulf of Lion.  
42 *J. Geophys. Res.*, 116.
- 43 Hu, Z. Y., Petrenko, A. A., Doglioli, A. M., and Dekeyser, I. (2011b). Study  
44 of mesoscale anticyclonic eddy in the western part of the Gulf of Lion.  
45 *J. Mar. Sys.*, 88:3–11.

- 1 Huthnance, J. (1995). Circulation, exchange and water masses at the ocean  
2 margin: the role of physical processes at the shelf edge. *Prog. Oceanogr.*,  
3 35(4):353 – 431.
- 4 Huthnance, J. M., Holt, J. T., and Wakelin, S. L. (2009). Deep ocean exchange  
5 with west-european shelf seas. *Ocean Sci.*, 5(4):621–634.
- 6 Huthnance, J. M., Van Aken, H. M., White, M., Barton, E. D., Le Cann, B.,  
7 Ferreira Coelho, E., Alvarez Fanjul, E., Miller, P., and Vitorino, J. (2002).  
8 Ocean margin exchange–water flux estimates. *J. Mar. Sys.*, 32(1-3):107 –  
9 137.
- 10 Johnson, J. and Chapman, P. (2011). Preface "Deep Ocean Exchange with  
11 the Shelf (DOES)". *Ocean Sci.*, 7(1).
- 12 Kersalé, M., Doglioli, A. M., Petrenko, A. A., Dekeyser, I., and Nencioli, F.  
13 (2013). Physical characteristics and dynamics of the coastal Latex09 Eddy  
14 derived from in situ data and numerical modeling. *J. Geophys. Res.*, 118:1–  
15 11.
- 16 Kersalé, M., Petrenko, A. A., Doglioli, A. M., Nencioli, F., Bouffard, J., Blain,  
17 S., Diaz, F., Labasque, T., Quéguiner, B., and Dekeyser, I. (2015). Lat-  
18 eral diffusivity coefficients from the dynamics of a SF6 patch in a coastal  
19 environment. *J. Mar. Sys.*, 153:42–54.
- 20 Kirincich, A. R. and Barth, J. A. (2009). Time-varying across-shelf ekman  
21 transport and vertical eddy viscosity on the inner shelf. *J. Phys. Oceanogr.*,  
22 39(3):602.
- 23 Law, C., Watson, A., and Liddicoat, M. (1994). Automated vacuum analysis  
24 of sulphur hexafluoride in seawater: derivation of the atmospheric trend  
25 (1970–1993) and potential as a transient tracer. *Mar. Chem.*, 48(1):57 – 69.
- 26 Ledwell, J. R. and Watson, A. J. (1991). The Santa-Monica Basin tracer  
27 experiment - A study of diapycnal and isopycnal mixing. *J. Geophys. Res.*,  
28 96(C5):8695–8718.
- 29 Ledwell, J. R., Watson, A. J., and Law, C. S. (1998). Mixing of a tracer in  
30 the pycnocline. *J. Geophys. Res.*, 103(C10):21499–21529.
- 31 Lehahn, Y., d’Ovidio, F., Lévy, M., and Heifetz, E. (2007). Stirring of the  
32 northeast atlantic spring bloom: A lagrangian analysis based on multisatel-  
33 lite data. *J. Geophys. Res.*, 112(C08005).
- 34 Lévy, M., Ferrari, R., Franks, P. J., Martin, A. P., and Rivière, P. (2012).  
35 Bringing physics to life at the submesoscale. *Geophys. Res. Lett.*, 39(14).
- 36 Lumpkin, R. and Elipot, S. (2010). Surface drifter pair spreading in the North  
37 Atlantic. *J. Geophys. Res.*, 115.
- 38 MacFadyen, A. and Hickey, B. M. (2010). Generation and evolution of a topo-  
39 graphically linked, mesoscale eddy under steady and variable wind-forcing.  
40 *Cont. Shelf Res.*, 30(13):1387–1402.
- 41 MacFadyen, A., Hickey, B. M., and Cochlan, W. P. (2008). Influences of the  
42 Juan de Fuca Eddy on circulation, nutrients, and phytoplankton production  
43 in the northern California Current System. *J. Geophys. Res.*, 113(C08008).
- 44 Mahadevan, A. (2016). The impact of submesoscale physics on primary pro-  
45 ductivity of plankton. *Ann. Rev. Mar. Sci.*, 8(1):161–184.

- 1 Mancho, A. M., Hernandez Garcia, E., Small, D., Wiggins, S., and Fernandez,  
2 V. (2008). Lagrangian transport through an ocean front in the northwestern  
3 Mediterranean sea. *J. Phys. Oceanogr.*, 38(6):1222–1237.
- 4 Marsaleix, P., Auclair, F., and Estournel, C. (2006). Considerations on Open  
5 Boundary Conditions for Regional and Coastal Ocean Models. *J. At-*  
6 *mos. Ocean. Technol.*, 23:1604–1613.
- 7 Marsaleix, P., Auclair, F., Floor, J., Herrmann, M., Estournel, C., Pairaud,  
8 I., and Ulses, C. (2008). Energy conservation issues in sigma-coordinate  
9 free-surface ocean models. *Ocean Model.*, 20:61–89.
- 10 McWilliams, J. C., Brown, E. D., Bryden, H. L., Ebbesmeyer, C. C., Elliott,  
11 B. A., Heinmiller, R. H., Lien Hua, B., Leaman, K. D., Lindstrom, E. J.,  
12 Luyten, J. R., McDowell, S. E., Breckner Owens, W., Perkins, H., Price,  
13 J. F., Regier, L., Riser, S. C., Rossby, H. T., Sanford, T. B., Shen, C. Y.,  
14 Taft, B. A., and Van Leer, J. C. (1983). *The Local Dynamics of Eddies*  
15 *in the Western North Atlantic*, pages 92–113. Springer Berlin Heidelberg,  
16 Berlin, Heidelberg.
- 17 Melson, A., Meyers, S. D., Hurlburt, H. E., Metzger, E. J., and O’Brien, J. J.  
18 (1999). ENSO effects on Gulf of Alaska eddies. *Earth Interactions* 3, 003.
- 19 Millot, C. (1979). Wind induced upwellings in the Gulf of Lions. *Oceanol. Acta*,  
20 2:261–274.
- 21 Millot, C. (1982). *Analysis of upwelling in the Gulf of Lions - Hydrodynam-*  
22 *ics of semi-enclosed seas: Proceedings of the 13th International Liège Col-*  
23 *loquium on Ocean Hydrodynamics.*, volume 34. Elsevier Oceanogr. Ser.,  
24 Amsterdam, The Netherlands.
- 25 Millot, C. (1990). The Gulf of Lions’ hydrodynamics. *Cont. Shelf Res.*, 10:885–  
26 894.
- 27 Millot, C. and Crépon, M. (1981). Inertial Oscillations on the Continental  
28 Shelf of the Gulf of Lions. *J. Phys. Oceanogr.*, 11:639–657.
- 29 Millot, C. and Taupier-Letage, I. (2005). Additional evidence of LIW en-  
30 trainment across the Algerian subbasin by mesoscale eddies and not by a  
31 permanent westward flow. *Prog. Oceanogr.*, 66(2):231–250.
- 32 Millot, C. and Wald, L. (1980). The effect of Mistral wind on the Ligurian  
33 current near Provence. *Oceanol. Acta*, 3(4):399–402.
- 34 Mitchelson-Jacob, G. and Sundby, S. (2001). Eddies of Vestfjorden, Norway.  
35 *Cont. Shelf Res.*, 21(16-17):1901–1918.
- 36 Moore II, T., Matear, R., Marra, J., and Clementson, L. (2007). Phytoplankton  
37 variability off the western Australian coast: Mesoscale eddies and their role  
38 in cross-shelf exchange. *Deep-Sea Res. II*, 54(8-10):943–960.
- 39 Moutin, T. and Bonnet, S. (2015). OUTPACE cruise, RV L’Atalante,  
40 <http://dx.doi.org/10.17600/15000900>.
- 41 Nagai, T., Gruber, N., Frenzel, H., Lachkar, Z., McWilliams, J. C., and Platt-  
42 tner, G.-K. (2015). Dominant Role of Eddies and Filaments in the Off-  
43 shore Transport of Carbon and Nutrients in the California Current System.  
44 *J. Geophys. Res.*, 120.
- 45 Naudin, J. J., Cauwet, G., Chretiennot-Dinet, M.-J., Deniaux, B., Devenon, J.-  
46 L., and Pauc, H. (1997). River discharge and wind influence upon particulate

- 1 transfer at the land–ocean interaction: case study of the Rhône river plume.  
2 *Estuar. Coast. Shelf S.*, 45(3):303–316.
- 3 Nencioli, F., d’Ovidio, F., Doglioli, A., and Petrenko, A. (2013). In situ es-  
4 timates of submesoscale horizontal eddy diffusivity across an ocean front.  
5 *J. Geophys. Res.*, 118(12):7066–7080.
- 6 Nencioli, F., d’Ovidio, F., Doglioli, A. M., and Petrenko, A. A. (2011). Sur-  
7 face coastal circulation patterns by in-situ detection of Lagrangian coherent  
8 structures. *Geophys. Res. Lett.*, 38(L17604).
- 9 Nencioli, F., Kuwahara, V. S., Dickey, T. D., Rii, Y. M., and Bidigare, R. R.  
10 (2008). Physical dynamics and biological implications of a mesoscale eddy  
11 in the lee of Hawai’i : Cyclone Opal observations during E-FLUX III. *Deep-*  
12 *Sea Res. II*, 55(10-13):1252–1274.
- 13 Nencioli, F., Petrenko, A. A., and Doglioli, A. M. (2016). Diagnosing cross-  
14 shelf transport along an ocean front: an observational case study in the Gulf  
15 of Lion. *J. Geophys. Res.*, (121):7218–7243.
- 16 Nof, D. (1999). Strange encounters of eddies with walls. *J. Mar. Res.*,  
17 57(5):739–761.
- 18 Olascoaga, M. J., Rypina, I. I., Brown, M. G., Beron Vera, F. J., Kocak, H.,  
19 Brand, L. E., Halliwell, G. R., and Shay, L. K. (2006). Persistent transport  
20 barrier on the West Florida Shelf. *Geophys. Res. Lett.*, 33(22).
- 21 Petrenko, A. A. (2003). Variability of circulation features in the Gulf of Lion  
22 NW Mediterranean Sea. Importance of inertial currents. *Oceanol. Acta*,  
23 26:323–338.
- 24 Petrenko, A. A. (2007). Latex00 cruise in the Gulf of Lion, RV Téthys II,  
25 <http://dx.doi.org/10.17600/7450130>.
- 26 Petrenko, A. A. (2008). Latex08 cruise in the Gulf of Lion, RV Téthys II,  
27 <http://dx.doi.org/10.17600/8450140>.
- 28 Petrenko, A. A. (2009). Latex09 cruise in the Gulf of Lion, RV Téthys II,  
29 <http://dx.doi.org/10.17600/9450140>.
- 30 Petrenko, A. A. (2010). Latex10 cruise in the Gulf of Lion, RV Téthys II,  
31 <http://dx.doi.org/10.17600/10450150>.
- 32 Petrenko, A. A., Dufau, C., and Estournel, C. (2008). Barotropic eastward cur-  
33 rents in the western Gulf of Lion, northwestern Mediterranean Sea, during  
34 stratified conditions. *J. Mar. Sys.*, 74(1-2):406–428.
- 35 Petrenko, A. A., Kersalé, M., Nencioli, F., Gatti, J., Doglioli, A. M., and  
36 Dekeyser, I. (2013). Coastal circulation in the Gulf of Lion, the influence  
37 of mesoscale processes on interregional exchanges. *40th CIESM Congress*  
38 *proceedings*.
- 39 Petrenko, A. A., Leredde, Y., and Marsaleix, P. (2005). Circulation in a strat-  
40 ified and wind-forced Gulf of Lions, NW Mediterranean Sea: in situ and  
41 modeling data. *Cont. Shelf Res.*, 25:7–27.
- 42 Pinardi, N. (2003). The Mediterranean ocean forecasting system : first phase  
43 of implementation (1998-2001). *Ann. Geophys.*, 21:3–20.
- 44 Quéguiner, B. (2011). KEOPS 2 cruise, RV Marion Dufresne,  
45 <http://dx.doi.org/10.17600/11200050>.

- 1 Reverdin, G., Morisset, S., Marié, L., Bourras, D., Sutherland, G., Ward,  
2 B., Salvador, J., Font, J., Cuypers, Y., Centurioni, L., Hormann, V.,  
3 Koldziejczyk, N., Boutin, J., D'Ovidio, F., Nencioli, F., Martin, N., Diverres,  
4 D., Alory, G., and Lumpkin, R. (2015). Surface salinity in the North At-  
5 lantic subtropical gyre during the STRASSE/SPURS summer 2012 cruise.  
6 *Oceanography*, 28:114–123.
- 7 Robinson, A. R. (1983). *Overview and Summary of Eddy Science*, pages 3–15.  
8 Springer Berlin Heidelberg, Berlin, Heidelberg.
- 9 Roughan, M., Garfield, N., Largier, J., Dever, E., Dorman, C., Peterson, D.,  
10 and Dorman, J. (2006). Transport and retention in an upwelling region:  
11 The role of across-shelf structure. *Deep Sea Res. II*, 53(25–26):2931–2955.
- 12 Ruiz, S., Pascual, A., Mahadevan, A., Claret, M., Olita, A., Troupin, C., Tin-  
13 toré, J., Poulain, P., Tovar-Sánchez, A., Mourre, B., and Capet, A. (2016).  
14 Intense ocean frontogenesis inducing submesoscale processes and impacting  
15 biochemistry. 48th International Liège Colloquium on Ocean Dynamics,  
16 Liège, Belgium. oral pres.
- 17 Schaeffer, A., Molcard, A., Forget, P., Fraunié, P., and Garreau, P. (2011).  
18 Generation mechanisms for mesoscale eddies in the Gulf of Lions : radar  
19 observation and modeling. *Ocean Dynam.*, 61:1587–1609.
- 20 Schroeder, K., Haza, A. C., Griffo, A., Özgökmen, T. M., Poulain, P. M.,  
21 Gerin, R., Peggion, G., and Rixen, M. (2011). Relative dispersion in the  
22 Liguro-Provençal basin: From sub-mesoscale to mesoscale. *Deep Sea Res. I*,  
23 58(3):209–228.
- 24 Shcherbina, A. Y., Sundermeyer, M. A., Kunze, E., D'Asaro, E., Badin, G.,  
25 Birch, D., Brunner-Suzuki, A.-M. E. G., Callies, J., Kuebel Cervantes, B. T.,  
26 Claret, M., Concannon, B., Early, J., Ferrari, R., Goodman, L., Harcourt,  
27 R. R., Klymak, J. M., Lee, C. M., Lelong, M.-P., Levine, M. D., Lien, R.-C.,  
28 Mahadevan, A., McWilliams, J. C., Molemaker, M. J., Mukherjee, S., Nash,  
29 J. D., Özgökmen, T., Pierce, S. D., Ramachandran, S., Samelson, R. M.,  
30 Sanford, T. B., Shearman, R. K., Skillingstad, E. D., Smith, K. S., Tandon,  
31 A., Taylor, J. R., Terray, E. A., Thomas, L. N., and Ledwell, J. R. (2015).  
32 The LatMix Summer Campaign: Submesoscale Stirring in the Upper Ocean.  
33 *Bull. Am. Met. Soc.*, 96(8):1257–1279.
- 34 Ssalto/Duacs User Handbook, C. N. E. S. (2010). (M)SLA and (M)ADT  
35 near-real time and delayed time products, CNES (Centre National d'Etudes  
36 Spatiales). Technical report. Ref. cLS-DOS-NT-06.034.
- 37 Staneva, J. V., Dietrich, D. E., Stanev, E. V., and Bowman, M. J. (2001).  
38 Rim current and coastal eddy mechanisms in an eddy-resolving Black Sea  
39 general circulation model. *J. Mar. Sys.*, 31(1):137–157.
- 40 Suthers, I. M., Young, J. W., Baird, M. E., Roughan, M., Everett, J. D., Brass-  
41 ington, G. B., Byrne, M., Condie, S. A., Hartog, J. R., and Hassler, C. S.  
42 (2011). The strengthening East Australian Current, its eddies and biological  
43 effects – an introduction and overview. *Deep-Sea Res. II*, 58(5):538–546.
- 44 Tew Kai, E., Rossi, V., Sudre, J., Weimerskirch, H., Lopez, C., Hernandez Gar-  
45 cia, E., Marsac, F., and Garçon, V. (2009). Top marine predators track La-  
46 grangian coherent structures. *Proc. Natl. Acad. Sci. U. S. A.*, 106(20):8245–

- 1 8250.
- 2 Thomas, L. N., Tandon, A., and Mahadevan, A. (2008). *Submesoscale Pro-*  
3 *cesses and Dynamics*, pages 17–38. American Geophysical Union.
- 4 Wanninkhof, R., Hitchcock, G., Wiseman, W. J., Vargo, G., Ortner, P. B.,  
5 Asher, W., Ho, D. T., Schlosser, P., Dickson, M.-L., Masserini, R., et al.  
6 (1997). Gas exchange, dispersion, and biological productivity on the west  
7 Florida shelf: Results from a Lagrangian tracer study. *Geophys. Res. Lett.*,  
8 24(14):1767–1770.
- 9 Waugh, D. W. and Abraham, E. R. (2008). Stirring in the global surface  
10 ocean. *Geophys. Res. Lett.*, 35(20).